Circular dichroism, magnetic knots, and the spectropolarimetry of the cosmic microwave background

Massimo Giovannini[*]

Department of Physics, Theory Division, CERN, 1211 Geneva 23, Switzerland
INFN, Section of Milan-Bicocca, 20126 Milan, Italy

When the last electron-photon scattering takes place in a magnetized environment, the degree of circular polarization of the outgoing radiation depends upon the magnetic field strength. After deriving the scattering matrix of the process, the generalized radiative transfer equations are deduced in the presence of the relativistic fluctuations of the geometry and for all the four brightness perturbations. The new system of equations is solved under the assumption that the incident radiation is not polarized. The induced *V*-mode polarization is analyzed both analytically and numerically. The corresponding angular power spectra are calculated and compared with the measured (or purported) values of the linear polarizations (i.e. *E* mode and *B* mode) as they arise in the concordance model and in its neighboring extensions. Possible connections between the *V*-mode polarization of the cosmic microwave background and the topological properties of the magnetic flux lines prior to equality are outlined and briefly explored in analogy with the physics of magnetized sunspots.

I. MOTIVATIONS AND GOALS

The circular polarization of the cosmic microwave background (CMB in what follows) is not the direct target of forthcoming experimental searches. It will be argued hereunder that more accurate spectropolarimetric measurements of the *V*-mode polarization can be enlightening especially as a diagnostic of the magnetization of the predecoupling plasma. The primary goal of experimental endeavors in the near future is related, in one way or another, to the determination of the angular power spectra of the intensity and of the linear polarization of the CMB radiation field. Even the *B*-mode polarization, one of the primary objectives of diverse experimental programs, will be unable to shed light on the circular polarizations of the CMB. To avoid possible misunderstandings on this point it is desirable to introduce the relevant conventions on the Stokes parameters of the radiation field[1]

$$I = |\vec{E} \cdot \hat{e}_1|^2 + |\vec{E} \cdot \hat{e}_2|^2, \qquad V = 2 \operatorname{Im}[(\vec{E} \cdot \hat{e}_1)^*(\vec{E} \cdot \hat{e}_2)], \tag{1.1}$$

$$\begin{aligned} Q &= |\vec{E} \cdot \hat{e}_1|^2 - |\vec{E} \cdot \hat{e}_2|^2, \\ U &= 2 \operatorname{Re}[(\vec{E} \cdot \hat{e}_1)^*(\vec{E} \cdot \hat{e}_2)], \end{aligned} \tag{1.2}$$

where $\hat{e}_1$ and $\hat{e}_2$ are two mutually orthogonal directions both perpendicular to the direction of propagation $\hat{n}$ which is chosen to lie along $\hat{e}_3$. The temperature autocorrelation

(i.e. the *TT* angular power spectrum[2]) stems directly from the brightness perturbation of the intensity of the radiation field: the fluctuations of the space-time curvature act as sources of inhomogeneity of the intensity. The treatment of the polarization is slightly more cumbersome and it has to do with the transformation properties of the Stokes parameters. Consider a rotation of the unit vectors $\hat{e}_1$ and $\hat{e}_2$ in the plane orthogonal to $\hat{n}$ and suppose that the rotation angle is φ. By rotating the axes in the right-handed sense, i.e. as

$$\hat{e}_1' = \cos\varphi \, \hat{e}_1 + \sin\varphi \, \hat{e}_2, \qquad \hat{e}_1' = -\sin\varphi \, \hat{e}_1 + \cos\varphi \, \hat{e}_2, \tag{1.3}$$

the Stokes parameters of Eq. (1.1) are left invariant (i.e. $I' = I$ and $V' = V$) while Q and U [introduced in Eq. (1.2)] transform as

$$\begin{aligned} Q' &= \cos 2\varphi \, Q + \sin 2\varphi \, U, \\ U' &= -\sin 2\varphi \, Q + \cos 2\varphi \, U. \end{aligned} \tag{1.4}$$

In other words, while I and V are invariant under a two-dimensional rotation, Q and U do transform and do mix under the same rotation. It is worth stressing that the transformation parametrized by Eq. (1.3) is not a global rotation of the coordinate system but it is rather a rotation on the tangent plane to the two-sphere at a given point. The transformation properties of the Stokes parameters under Eq. (1.3) allow one determine their associated spin weight [4–7]. The brightness perturbations associated with I and V

---

*massimo.giovannini@cern.ch
[1]From the definitions of the Stokes parameters it follows (see, e.g. [1–3]) that $I^2 \geq Q^2 + U^2 + V^2$, where the equality sign arises in the case of the field of a plane wave.

[2]The specific definitions of the relevant angular power spectra are provided hereunder, see, e.g. Eqs. (1.11) and (1.12).

(i.e. Δ_I and Δ_V) both have spin weight 0. The brightness perturbations of Q and U (i.e. Δ_Q and Δ_U) transform as a function of spin weight ± 2, since, from Eq. (1.4), $\Delta_\pm(\hat{n}, \tau) = \Delta_Q(\hat{n}, \tau) \pm i\Delta_U(\hat{n}, \tau)$ transform as $\Delta'_\pm(\hat{n}, \tau) = e^{\mp 2i\varphi}\Delta_\pm(\hat{n}, \tau)$. Consequently, while $\Delta_\pm(\hat{n}, \tau)$ have to be expanded, on the two-sphere, in terms of spin-± 2 spherical harmonics $_{\pm 2}Y_{\ell m}(\hat{n})$

$$\Delta_\pm(\hat{n}, \tau) = \sum_{\ell m} a_{\pm 2, \ell m \pm 2}Y_{\ell m}(\hat{n}), \qquad (1.5)$$

$\Delta_I(\hat{n}, \tau)$ and $\Delta_V(\hat{n}, \tau)$ have to be expanded on the basis of spherical harmonics $Y_{\ell m}(\hat{n})$ as:

$$\Delta_I(\hat{n}, \tau) = \sum_{\ell m} a_{\ell m}^{(I)}Y_{\ell m}(\hat{n}), \qquad \Delta_V(\hat{n}, \tau) = \sum_{\ell m} a_{\ell m}^{(V)}Y_{\ell m}(\hat{n}). \qquad (1.6)$$

Both spin-0 and spin-± 2 spherical harmonics arise naturally as Wigner matrix elements [8] depending in general upon three different eigenvalues: while the third eigenvalue is 0 for scalar harmonics, it is $\mp s$ for spin-s weighted harmonics. The complete information on the radiation field of the CMB should therefore stem from the analysis of the TT and VV angular power spectra

$$C_\ell^{(TT)} = \frac{1}{2\ell + 1} \sum_{m=-\ell}^{\ell} \langle a_{\ell m}^{(I)*} a_{\ell m}^{(I)} \rangle,$$
$$C_\ell^{(VV)} = \frac{1}{2\ell + 1} \sum_{m=-\ell}^{\ell} \langle a_{\ell m}^{(V)*} a_{\ell m}^{(V)} \rangle, \qquad (1.7)$$

as well as from the angular power spectra of the E-mode and B-mode autocorrelations.[3] The E-mode and B-mode autocorrelations are defined as

$$C_\ell^{(EE)} = \frac{1}{2\ell + 1} \sum_{m=-\ell}^{\ell} \langle a_{\ell m}^{(E)*} a_{\ell m}^{(E)} \rangle,$$
$$C_\ell^{(BB)} = \frac{1}{2\ell + 1} \sum_{m=-\ell}^{\ell} \langle a_{\ell m}^{(B)*} a_{\ell m}^{(B)} \rangle, \qquad (1.8)$$

where $a_{\ell m}^{(E)}$ and $a_{\ell m}^{(B)}$ are a linear combination of the coefficients $a_{\pm 2, \ell m}$ already introduced in Eq. (1.5):

$$a_{\ell m}^{(E)} = -\frac{1}{2}(a_{2, \ell m} + a_{-2, \ell m}),$$
$$a_{\ell m}^{(B)} = \frac{i}{2}(a_{2, \ell m} - a_{-2, \ell m}). \qquad (1.9)$$

In real space the fluctuations constructed from $a_{\ell m}^{(E)}$ and $a_{\ell m}^{(B)}$ have the property of being invariant under rotations on a plane orthogonal to $\hat{n}$ and, up to an ℓ-dependent prefactor, they can be expanded in terms of (ordinary) spherical harmonics:

$$\Delta_E(\hat{n}, \tau) = \sum_{\ell m} N_\ell^{-1} a_{\ell m}^{(E)}Y_{\ell m}(\hat{n}),$$
$$\Delta_B(\hat{n}, \tau) = \sum_{\ell m} N_\ell^{-1} a_{\ell m}^{(B)}Y_{\ell m}(\hat{n}), \qquad (1.10)$$

where $N_\ell = \sqrt{(\ell - 2)!/(\ell + 2)!}$. Before matter radiation equality the radiation field is customarily assumed to be unpolarized. The properties of electron-photon (and ion-photon) scattering imply that the radiation can become linearly polarized provided the incident brightness perturbations have a nonvanishing quadrupole moment,[4] i.e. $\Delta_{I2} \neq 0$.

Circular dichroism as well as linear polarization of the CMB becomes theoretically plausible in the presence of preequality magnetic fields [9,10] but, so far, there has not been any specific calculation of the circular polarization induced by a magnetized plasma prior to recombination and in the framework of the concordance model. One of the purposes of this article is to fill such a gap. While the V-mode polarization is suppressed in comparison with the E-mode polarization, the question is to determine quantitatively the nature of the suppression and its typical range in multipole space. The answer to the latter question can only be dynamical: it will be interesting, for the present purposes, to understand how, when and to what extent a radiation field which is originally unpolarized prior to equality will become circularly polarized after photon decoupling.

Some of the phenomenological aspects of the present considerations can be understood in analogy with solar spectropolarimetry. The knowledge of large-scale magnetism is often inspired (and partially modeled) by our improved understanding of solar magnetism (see, for instance, [11] for a dedicated review on the subject). Circular polarization is known to occur in sunspots [12–14] and it is sometimes argued that the analysis of polarization might improve the understanding of the local topology of magnetic flux lines in the vicinity of sunspots [11]. The amount of circular polarization depends, in the case of the sun, both on the gradients of the velocity field as well as upon the magnetic field topology and intensity. A naive approach to the problem would suggest that, absent any velocity gradient, $V \simeq 9 \times 10^{-12}B_{\text{spot}}\lambda I$ where λ is the wavelength in units of nm (1 nm $= 10^{-9}$ m) and B_{spot} is the magnetic field in units of gauss. As noted long ago (see

---

[3]This statement on the autocorrelations of temperature and polarization does not exclude the possibility of discussing and measuring the various cross correlations between temperature and polarization.

[4]As usual $\Delta_{I\ell}$ denotes the ℓth multipole of the intensity of the radiation field. With the same notation we will refer, when needed, to the multipoles of other observables.

e.g. [12,13]) for typical values of the magnetic field (i.e. $B_{spot} \sim$ kG) and for optical wavelengths (i.e. $380 < \lambda < 750$ nm) we would get $V/I \sim 10^{-5}$ which is 1 or 2 orders of magnitude smaller than what is approximately observed. The latter discrepancy suggested (see e.g. [15]) the important role played by velocity gradients whose contribution should be included for a consistent interpretation of the observational data.

Circular polarization arises naturally also in synchrotron emission [16–18] (see also [19,20]). In this second context the amount of circular polarization is generated from the linear polarization by the so-called Faraday conversion effect. In the case of the CMB the relativistic effect associated with the synchrotron emission is difficult to realize. On the contrary the predecoupling plasma is rather cold and the electrons are nonrelativistic. Furthermore, it is difficult to justify that the initial radiation field should be linearly polarized already well before equality. The only way Faraday conversion could lead to circular polarization is as a secondary effect when the linearly polarized CMB photons impinge on the relativistic electrons in the cluster magnetic field [21]. In this paper, on the contrary, the target is to compute the amount of circular polarization induced at early times by a predecoupling magnetic field and in terms of unpolarized initial conditions of the Einstein-Boltzmann hierarchy. To introduce some quantitative (but still general) considerations it is practical to define, for immediate convenience,

$$G_{\ell}^{(TT)} = \frac{\ell(\ell + 1)}{2\pi} C_{\ell}^{(TT)}, \qquad G_{\ell}^{(VV)} = \frac{\ell(\ell + 1)}{2\pi} C_{\ell}^{(VV)},$$
$$(1.11)$$

$$G_{\ell}^{(EE)} = \frac{\ell(\ell + 1)}{2\pi} C_{\ell}^{(EE)}, \qquad G_{\ell}^{(BB)} = \frac{\ell(\ell + 1)}{2\pi} C_{\ell}^{(BB)},$$
$$(1.12)$$

measuring, for a given observable, the angular power per logarithmic interval of ℓ. With the same notation the cross correlations between different observables can be defined, for instance, as $G_{\ell}^{(TE)}$, $G_{\ell}^{(VT)}$ and so on and so forth. In terms of Eqs. (1.11) and (1.12) the typical orders of magnitude angular power spectra can then be summarized as[5]

$$G_{\ell}^{(TT)} \simeq \mathcal{O}(5 \times 10^3) \, (\mu K)^2,$$
$$G_{\ell}^{(TE)} \simeq \mathcal{O}(150) \, (\mu K)^2, \qquad (1.13)$$
$$G_{\ell}^{(EE)} \simeq \mathcal{O}(50) \, (\mu K)^2.$$

The TT and TE correlations have been accurately assessed by the WMAP Collaboration [22–24] (see also [25,26]). Interesting measurements on the EE correlations have been reported, for instance, by the QUaD experiment [27–30].

Other measurements on the TT correlation for large multipoles (i.e. $\ell > 1000$) have been reported by the ACBAR experiment [31,32]. While all the current experimental data are consistent with the standard ΛCDM paradigm they can also be used to estimate the parameters of a putative magnetized background. In this respect, the result is that large-scale magnetic fields of nG strength and slightly blue spectral indices are allowed by current CMB data [33,34]. The estimation of the parameters of a magnetized background led to the first estimate of the likelihood contours in the two-dimensional plane characterized by the magnetic spectral index and by the magnetic field intensity. In a frequentist perspective the results of [33,34] exclude, to 95% confidence level, a sizable portion of the parameter space of magnetized models centered around comoving field intensities of 3.2 nG and magnetic spectral indices[6] $n_B = 1.6$. The latter results hold when the underlying model is just the ΛCDM (concordance) paradigm[7] but the addition of, for instance, dark energy fluctuations does not change quantitatively the exclusion plots [35].

The B-mode polarization has not been measured yet and upper limits exist by various experiments. In the standard ΛCDM paradigm with no tensors the BB power spectrum vanishes. For instance magnetic fields of $\mathcal{O}(5 \text{ nG})$ and blue spectral index lead, at intermediate scales, to an angular power spectrum which can be as large as $10^{-3} \, (\mu K)^2$ [36]. The latter estimate can be compared, for instance, with the BB angular power spectrum expected from the tensor modes of the geometry and from the gravitational lensing of the CMB anisotropies. The tensor modes are the conventional (potential) source of B-mode polarization in the simplest extension of the ΛCDM paradigm. Defining r_T as the tensor to scalar ratio, a typical value $r_T \sim 0.3$ would imply, at intermediate multipoles (i.e. $\ell < 100$) a BB angular power spectrum of the order of $10^{-2} \, (\mu K)^2$.

The degree of circular polarization computed here depends, in the simplest case, upon the amount of curvature perturbations, upon the magnetic field parameters and upon the typical frequency of the experiment. For nG magnetic fields and for a reference frequency $\mathcal{O}(10)$ GHz the VV angular power spectrum is $G_{\ell}^{(VV)} \simeq 10^{-15} \, (\mu K)^2$. For the same range of parameters the cross correlation $G_{\ell}^{(VT)} \simeq 10^{-6.5} \, (\mu K)^2$. If the observational frequency decreases the signals can be larger. While this comparison will be more carefully performed in Sec. IV it is important to appreciate that, in some sense, the absolute magnitude of the different correlation functions represents just a necessary but insufficient guide for the observer since the sys-

---

[5]For sake of simplicity the numerical values quoted here refer to the maximum of each power spectrum.

[6]The conventions on the magnetic spectral indices n_B are exactly the same as the ones employed for the spectral index of curvature perturbations (denoted as n_s). The scale-invariant value corresponds, in both cases, to 1.

[7]In the acronym Λ stands for the (nonfluctuating) dark energy component while CDM stands for cold dark matter.

tematics associated with the circular polarization are different from the ones arising in the case of a linearly polarized signal [37]. The second point we wish to stress is that, as it will be apparent from the subsequent analysis, low frequency instruments seem to be experimentally preferable [38,39] and, in this respect, it is tempting to speculate that very low frequency (radio) techniques could be appropriately adapted [40–42]. The third point related to the potential observations of the effects is that spectropolarimetric techniques should probably be employed given the necessity of a simultaneous determination of the brightness perturbation of the intensity and of the V-mode polarization (see, in this respect, Sec. IV).

The analogy of the present problem with the physics of the sunspots suggests the possibility of connecting the amount of (measured) circular polarization with the topology of the magnetic flux lines. This topic is, in principle, rather rich and, in this paper, we will merely scratch the surface by presenting some particular examples which are only semirealistic and which are borrowed from known examples in plasma physics. Indeed, the study of the topology of magnetic flux lines has a long history going back to the pioneering work of Fermi and Chandrasekhar on the gravitational stability of the galactic arm [43,44]. It would be interesting, in perspective, to connect the possible occurrence (or absence) of the circular polarization with magnetized plasmas which minimize the magnetic energy while the helicity is conserved (as it should) at high conductivity (see, along this line, the seminal papers of Chandrasekhar, Kendall and Woltjer [45–47]).

The layout of the paper is the following. In Sec. II the photon-electron and photon-ion scattering will be discussed in the presence of a magnetic field in the guiding center approximation. Details are also reported in Appendix A. In Sec. III the same problem will be addressed in the case of a magnetic knot, i.e. a simple example of static configuration minimizing the energy at a fixed value of the magnetic helicity. It will be speculated that the degree of circular polarization could be eventually connected with the topological properties of the magnetic flux lines in the plasma. In Sec. IV the evolution equations of the brightness perturbations will be deduced and solved both analytically and numerically. Relevant details on this topic are given in Appendix B. The tight-coupling approximation will be applied to the new framework and analytical results for the V-mode power spectra for large angular scales will be derived. For smaller angular scales numerical results will also be presented and compared with the temperature and (linear) polarization anisotropies. Section V contains the concluding considerations.

II. MAGNETIZED ELECTRON-PHOTON SCATTERING

The electron-photon scattering is customarily computed without taking into account the contribution of the mag-

netic field itself to the scattering matrix. This happens not only in the case when magnetic fields are assumed to be absent but also in the presence of large-scale magnetic fields (see, for instance,[8] [48–50]). The purpose of this section is to drop such an assumption and to derive the appropriate scattering matrix for electron-photon scattering in a weakly magnetized plasma. It is practical to define, for the present purposes, the outgoing and ingoing Stokes vectors whose components are the Stokes parameters, i.e.

$$\mathcal{I}^{\text{out}}(\omega, \mu, \mu', \varphi, \varphi') = (I_1, I_2, U, V), \qquad (2.1)$$

$$\mathcal{I}^{\text{in}}(\omega, \mu', \varphi') = (I'_1, I'_2, U', V'), \qquad (2.2)$$

$\mu = \cos\vartheta$ and $\mu' = \cos\vartheta'$. The intensity I and one of the components of the linear polarization (i.e. Q) have been replaced, as usual, by $I_1 = (I + Q)/2$ and $I_2 = (I - Q)/2$. The components of the ingoing Stokes parameters have been distinguished by a prime and they depend upon $\mu' = \cos\vartheta'$ and φ'. The Stokes parameters depend upon the (angular) frequency $\omega = 2\pi\nu$. By definition, the scattering matrix connects the outgoing to the ingoing Stokes parameters as:

$$\mathcal{I}^{\text{out}}_i(\omega, \mu, \mu', \varphi, \varphi') = \mathcal{S}_{ij}(\omega, \mu, \mu', \varphi, \varphi')\mathcal{I}^{\text{in}}_j(\omega, \mu', \varphi'). \tag{2.3}$$

The coordinate system has been fixed as[9]:

$$\hat{r} = (\cos\varphi \sin\vartheta, \cos\varphi \sin\vartheta, \cos\vartheta), \qquad (2.4)$$

$$\hat{\theta} = (\cos\varphi \cos\vartheta, \sin\varphi \cos\vartheta, -\sin\vartheta), \qquad (2.5)$$

$$\hat{\varphi} = (-\sin\varphi, \cos\varphi, 0). \qquad (2.6)$$

The purpose is to obtain the scattering matrix of electron-photon scattering (see, e.g. [2]) but in the presence of a magnetic field and in the guiding center approximation [51] which is, in practice, a controlled expansion in gradients of the magnetic field intensity. The derivation of the various components of the scattering matrix is reported in Appendix A. In what follows only the results will be reported and discussed. Defining as $r_e = e^2/m_e$ the classical radius of the electron, the various components of the scattering matrix can be written as:

---

[8]It is appropriate to stress that it would be rather pretentious to give a complete and thorough list of references in connection with primordial magnetism. The easiest solution is to refer the interested reader to the dedicated review articles of [9,10] where a more complete bibliography can be found.

[9]The orientation of the coordinate system corresponding to Eqs. (2.4)–(2.6) implies that $\hat{\vartheta} \times \hat{\varphi} = \hat{r}$. In other classic references such as [2] the orientation is such that $\hat{\vartheta} \times \hat{\varphi} = -\hat{r}$; this different choice entails a modification of Eq. (2.6), i.e. $\hat{\varphi} = (\sin\varphi, -\cos\varphi, 0)$. The conventions spelled out by Eqs. (2.4)–(2.6) will be followed throughout the paper.

$$S_{11} = \frac{r_e^2}{2r^2}\{2\Lambda_3(\omega)(1-\mu^2)(1-\mu'^2)$$
$$+ \zeta^2(\omega)\mu^2\mu'^2[1+f_e^2(\omega)\Lambda_2^2(\omega)]$$
$$- 4\zeta(\omega)\Lambda_3(\omega)\mu\mu'\sqrt{1-\mu^2}\sqrt{1-\mu'^2}$$
$$\times \cos(\varphi'-\varphi) + \zeta^2(\omega)[1-f_e^2(\omega)\Lambda_2^2(\omega)]$$
$$\times \mu^2\mu'^2\cos[2(\varphi'-\varphi)]\}, \tag{2.7}$$

$$S_{12} = \frac{\mu^2\zeta^2(\omega)r_e^2}{2r^2}\{1+f_e^2(\omega)\Lambda_2^2(\omega)$$
$$- [1-f_e^2(\omega)\Lambda_2^2(\omega)]\cos[2(\varphi'-\varphi)]\}, \tag{2.8}$$

$$S_{13} = \frac{r_e^2}{r^2}\{\zeta(\omega)\Lambda_3(\omega)\mu\sqrt{1-\mu^2}\sqrt{1-\mu'^2}\sin(\varphi'-\varphi)$$
$$- \frac{1}{2}\zeta^2(\omega)\mu^2\mu'[1-f_e^2(\omega)]\sin[2(\varphi'-\varphi)]\}, \tag{2.9}$$

$$S_{14} = \frac{r_e^2 f_e(\omega)\zeta(\omega)\Lambda_2(\omega)}{r^2}\mu[\zeta(\omega)\mu\mu'-\Lambda_3(\omega)$$
$$\times \sqrt{1-\mu^2}\sqrt{1-\mu'^2}\cos(\varphi'-\varphi)], \tag{2.10}$$

$$S_{21} = \frac{\zeta^2(\omega)\mu'^2 r_e^2}{2r^2}\{\Lambda_1^2(\omega)+f_e^2(\omega)\Lambda_2^2(\omega)$$
$$- [\Lambda_1^2(\omega)-f_e^2(\omega)\Lambda_2^2(\omega)]\cos[2(\varphi'-\varphi)]\}, \tag{2.11}$$

$$S_{22} = \frac{\zeta^2(\omega)r_e^2}{2r^2}\{\Lambda_1^2(\omega)+f_e^2(\omega)\Lambda_2^2(\omega)$$
$$+ [\Lambda_1^2(\omega)-f_e^2(\omega)\Lambda_2^2(\omega)]\cos[2(\varphi'-\varphi)]\}, \tag{2.12}$$

$$S_{23} = \frac{\zeta^2(\omega)r_e^2}{2r^2}[\Lambda_1^2(\omega)-f_e^2(\omega)\Lambda_2^2(\omega)]\mu'\sin[2(\varphi'-\varphi)], \tag{2.13}$$

$$S_{24} = \frac{r_e^2}{r^2}f_e(\omega)\zeta^2(\omega)\Lambda_1(\omega)\Lambda_2(\omega)\mu', \tag{2.14}$$

$$S_{31} = \frac{r_e^2}{r^2}\{-2\zeta(\omega)\Lambda_1(\omega)\Lambda_3(\omega)\sqrt{1-\mu^2}\mu'\sqrt{1-\mu'^2}$$
$$\times \sin(\varphi'-\varphi)$$
$$+ \zeta^2(\omega)\mu\mu'^2[\Lambda_1(\omega)-f_e^2(\omega)\Lambda_2^2(\omega)]$$
$$\times \sin[2(\varphi'-\varphi)]\}, \tag{2.15}$$

$$S_{32} = -\frac{r_e^2}{r^2}\zeta^2(\omega)[\Lambda_1(\omega)-f_e^2(\omega)\Lambda_2^2(\omega)]\mu\sin[2(\varphi'-\varphi)], \tag{2.16}$$

$$S_{33} = \frac{\zeta(\omega)r_e^2}{r^2}\{-\Lambda_1(\omega)\Lambda_3(\omega)\sqrt{1-\mu^2}\sqrt{1-\mu'^2}$$
$$\times \cos(\varphi'-\varphi) + \zeta(\omega)[\Lambda_1(\omega)-f_e^2(\omega)\Lambda_2^2(\omega)]\mu\mu'$$
$$\times \cos[2(\varphi'-\varphi)]\}, \tag{2.17}$$

$$S_{34} = -\frac{r_e^2}{r^2}f_e(\omega)\zeta(\omega)\Lambda_2(\omega)\Lambda_3(\omega)$$
$$\times \sqrt{1-\mu^2}\sqrt{1-\mu'^2}\sin(\varphi'-\varphi), \tag{2.18}$$

$$S_{41} = -\frac{r_e^2 f_e(\omega)\zeta(\omega)\Lambda_2(\omega)\mu'}{r^2}\{2\Lambda_3(\omega)\sqrt{1-\mu^2}\sqrt{1-\mu'^2}$$
$$\times \cos(\varphi'-\varphi)$$
$$- \zeta(\omega)\mu\mu'[\Lambda_1(\omega)+1-(\Lambda_1(\omega)-1)$$
$$\times \cos[2(\varphi'-\varphi)]]\}, \tag{2.19}$$

$$S_{42} = \frac{r_e^2 f_e(\omega)\zeta^2(\omega)\Lambda_2(\omega)\mu}{r^2}\{1+\Lambda_1(\omega)+[\Lambda_1(\omega)-1]$$
$$\times \cos[2(\varphi'-\varphi)]\}, \tag{2.20}$$

$$S_{43} = \frac{r_e^2}{r^2}\{f_e(\omega)\zeta(\omega)\Lambda_2(\omega)\Lambda_3(\omega)\sqrt{1-\mu^2}\sqrt{1-\mu'^2}$$
$$\times \sin(\varphi'-\varphi) - f_e(\omega)\zeta^2(\omega)\Lambda_2(\omega)$$
$$\times \mu\mu'[1-\Lambda_1(\omega)]\sin[2(\varphi'-\varphi)]\}, \tag{2.21}$$

$$S_{44} = \frac{r_e^2}{r^2}\{\mu\mu'\zeta^2(\omega)[\Lambda_1(\omega)+f_e^2(\omega)\Lambda_2^2(\omega)]$$
$$- \zeta(\omega)\Lambda_1(\omega)\Lambda_3(\omega)\sqrt{1-\mu^2}\sqrt{1-\mu'^2}$$
$$\times \cos(\varphi'-\varphi)\}. \tag{2.22}$$

In Eqs. (2.7)–(2.22) various (frequency dependent) quantities have been introduced, namely $f_e(\omega)$, $\Lambda_1(\omega)$, $\Lambda_2(\omega)$ and $\Lambda_3(\omega)$. Their explicit expressions are

$$\Lambda_1(\omega) = 1 + \left(\frac{\omega_{pi}^2}{\omega_{pe}^2}\right)\left(\frac{\omega^2-\omega_{Be}^2}{\omega^2-\omega_{Bi}^2}\right), \tag{2.23}$$

$$\Lambda_2(\omega) = 1 - \left(\frac{\omega_{pi}^2}{\omega_{pe}^2}\right)\left(\frac{\omega_{Bi}}{\omega_{Be}}\right)\left(\frac{\omega^2-\omega_{Be}^2}{\omega^2-\omega_{Bi}^2}\right), \tag{2.24}$$

$$\Lambda_3(\omega) = 1 + \left(\frac{\omega_{pi}^2}{\omega_{pe}^2}\right), \tag{2.25}$$

$$\zeta(\omega) = \frac{1}{f_e^2(\omega)-1} = \frac{\omega^2}{\omega_{Be}^2-\omega^2}, \qquad f_e(\omega) = \left(\frac{\omega_{Be}}{\omega}\right), \tag{2.26}$$

where $\omega_{Be,i}$ and $\omega_{pe,i}$ are the Larmor and plasma frequencies for electrons and ions, namely:

$$\omega_{Be} = \frac{eB}{m_e a}, \qquad \omega_{Bi} = \frac{eB}{m_p a}, \qquad (2.27)$$

$$\omega_{pe} = \sqrt{\frac{4\pi e^2 n_0}{m_e a(\tau)}}, \qquad \omega_{pi} = \sqrt{\frac{4\pi e^2 n_0}{m_p a(\tau)}}, \qquad (2.28)$$

where B is the modulus of the magnetic field intensity coinciding, in practice, with the lowest order result of the guiding center approximation. As discussed in Appendix A, Eqs. (2.27) and (2.28) take into account the redshift dependence of the frequency. The magnetic field appearing in Eq. (2.27) is the comoving magnetic field (see Appendix A) and this means, in particular, that the relation to the physical frequencies is given by

$$\omega_{Be} = \frac{e\mathcal{B}}{m_e} a(\tau) = \omega_{Be}^{\text{phys}} a(\tau), \qquad (2.29)$$

and similarly for the other quantities of Eqs. (2.27) and (2.28). The logic behind the functions defined in Eqs. (2.23)–(2.25) is that we want to factorize the electron contribution by keeping track of the ions. According to this strategy, to leading order in the ion contributions, $\Lambda_1(\omega)$, $\Lambda_2(\omega)$ and $\Lambda_3(\omega)$ turn out to be

$$\Lambda_1(\omega) = 1 + \mathcal{O}\left(\frac{m_e}{m_p}\right)\left[1 + \mathcal{O}\left(\frac{\omega_{Be}}{\omega}\right)\right],$$

$$\Lambda_2(\omega) = 1 - \mathcal{O}\left(\frac{m_e^2}{m_p^2}\right)\left[1 + \mathcal{O}\left(\frac{\omega_{Be}}{\omega}\right)\right], \qquad (2.30)$$

$$\Lambda_2(\omega) = 1 + \mathcal{O}\left(\frac{m_e}{m_p}\right).$$

In the limit $f_e(\omega) \to 0$ and by correspondingly setting $\Lambda_1(\omega) = \Lambda_2(\omega) = \Lambda_3(\omega) = 1$, Eqs. (2.7)–(2.22) reproduce exactly the results of Ref. [2] modulo the different orientation of the coordinate system [see Eqs. (2.4)–(2.6) and footnote therein] which leads to an overall sign difference in the matrix elements containing the sines. In the limit $\Lambda_1(\omega) = \Lambda_2(\omega) = \Lambda_3(\omega) \to 1$ the present results coincide with Ref. [52] (see also [53] modulo the typo pointed out in [52]). The evolution equations for the brightness perturbations can be written, in general terms, as[10]

$$\Delta_I' + \epsilon'\Delta_I + n^i\partial_i\Delta_I = \psi' - n^i\partial_i\phi + \epsilon'\mu v_b$$
$$+ \epsilon'C_I(\mu, \omega), \qquad (2.31)$$

_____

[10]Note the presence of the Doppler term arising in the source term of the intensity. The collisionless part of the evolution of the intensity perturbations is well known. For the interested reader it is derived, within the present conventions, in Ref. [54] and within different gauge choices.

$$\Delta_Q' + \epsilon'\Delta_Q + n^i\partial_i\Delta_Q = \epsilon'C_Q(\mu, \omega), \qquad (2.32)$$

$$\Delta_U' + \epsilon'\Delta_U + n^i\partial_i\Delta_U = \epsilon'C_U(\mu, \omega), \qquad (2.33)$$

$$\Delta_V' + \epsilon'\Delta_V + n^i\partial_i\Delta_V = \epsilon'C_V(\mu, \omega). \qquad (2.34)$$

Concerning Eqs. (2.31)–(2.34) a few comments are in order. The brightness perturbations can be classified in terms of their transformation properties under rotations in the three-dimensional Euclidean submanifold. This means that all the brightness perturbations will have a scalar, a vector and a tensor contribution. In the framework of the ΛCDM scenario the tensor and the vector fluctuations of the geometry are totally absent. Therefore, since we want to compute the circular polarization in the minimal situation, we will stick to the scalar modes of the geometry which are connected with the scalar modes of the brightness perturbations. As implied by the concordance model the background metric is taken to be conformally flat with signature mostly minus, i.e. $\bar{g}_{\mu\nu} = a^2(\tau)\eta_{\mu\nu}$ where $\eta_{\mu\nu} = \text{diag}(1, -1, -1, -1)$ is the Minkowski metric. In Eq. (2.31), ϕ and ψ represent the scalar fluctuations of the metric in the conformally Newtonian gauge, i.e. $\delta_s g_{00} = 2a^2\phi$ and $\delta_s g_{ij} = 2a^2\delta_{ij}\psi$. Always in Eq. (2.31), v_b is related to the baryon velocity (see Appendix A) i.e. the center of mass velocity of the electron-ion system. In Eqs. (2.31)–(2.34) ϵ' denotes, as usual, the differential optical depth, i.e.

$$\epsilon' = x_e\tilde{n}_e\sigma_{\gamma e}\frac{a}{a_0}, \qquad \sigma_{\gamma e} = \frac{8}{3}\pi r_e^2. \qquad (2.35)$$

After integration over φ' the source terms appearing in Eqs. (2.31)–(2.34) can be written as

$$C_I(\mu, \omega) = \frac{3\epsilon'}{16\pi}\int_{-1}^{1} d\mu'\{[\bar{P}_{11} + \bar{P}_{12} + \bar{P}_{21} + \bar{P}_{22}]$$
$$\times \Delta_I(\mu, \mu') + [\bar{P}_{11} - \bar{P}_{12} + \bar{P}_{21} - \bar{P}_{22}]$$
$$\times \Delta_Q(\mu, \mu') + 2[\bar{P}_{13} + \bar{P}_{23}]\Delta_U(\mu, \mu')$$
$$+ 2[\bar{P}_{14} + \bar{P}_{24}]\Delta_V(\mu, \mu')\}, \qquad (2.36)$$

$$C_Q(\mu, \omega) = \frac{3\epsilon'}{16\pi}\int_{-1}^{1} d\mu'\{[\bar{P}_{11} + \bar{P}_{12} - \bar{P}_{21} - \bar{P}_{22}]$$
$$\times \Delta_I(\mu, \mu') + [\bar{P}_{11} - \bar{P}_{12} - \bar{P}_{21} + \bar{P}_{22}]$$
$$\times \Delta_Q(\mu, \mu') + 2[\bar{P}_{13} - \bar{P}_{23}]\Delta_U$$
$$+ 2[\bar{P}_{14} - \bar{P}_{24}]\Delta_V(\mu, \mu')\}, \qquad (2.37)$$

$$C_U(\mu, \omega) = \frac{3\epsilon'}{16\pi} \int_{-1}^{1} d\mu' \{[\bar{P}_{31} + \bar{P}_{32}]\Delta_I(\mu, \mu')$$
$$+ [\bar{P}_{31} - \bar{P}_{32}]\Delta_Q(\mu, \mu') + 2\bar{P}_{33}\Delta_U(\mu, \mu')$$
$$+ 2\bar{P}_{34}\Delta_v(\mu, \mu')\}, \tag{2.38}$$

$$C_V(\mu, \omega) = \frac{3\epsilon'}{16\pi} \int_{-1}^{1} d\mu' \{[\bar{P}_{41} + \bar{P}_{42}]\Delta_I(\mu, \mu')$$
$$+ [\bar{P}_{41} - \bar{P}_{42}]\Delta_Q(\mu, \mu') + \bar{P}_{43}\Delta_U(\mu, \mu')$$
$$+ \bar{P}_{44}\Delta_V(\mu, \mu')\}, \tag{2.39}$$

where the generic matrix element appearing in Eqs. (2.36)–(2.39) is the integral over φ' of the corresponding element of the scattering matrix of Eq. (2.3), i.e.

$$\bar{P}_{ij}(\mu, \mu') = \int_0^{2\pi} \mathcal{S}_{ij}(\mu, \mu', \varphi') d\varphi'. \tag{2.40}$$

For immediate convenience it is appropriate to write down the explicit form of the various matrix elements appearing in Eqs. (2.36)–(2.39):

$$\bar{P}_{11}(\omega, \mu, \mu') = \pi\{2\Lambda_3(\omega)(1 - \mu^2)(1 - \mu'^2)$$
$$+ \zeta^2(\omega)\mu^2\mu'^2[1 + f_e^2(\omega)\Lambda_2^2(\omega)]\},$$
$$\bar{P}_{12}(\omega, \mu, \mu') = \pi\mu^2\zeta^2(\omega)[1 + f_e^2(\omega)\Lambda_2^2(\omega)],$$
$$\bar{P}_{13}(\omega, \mu, \mu') = 0,$$
$$\bar{P}_{14}(\omega, \mu, \mu') = 2\pi f_e(\omega)\zeta^2(\omega)\Lambda_2(\omega)\mu^2\mu',$$
$$\bar{P}_{21}(\omega, \mu, \mu') = \pi\zeta^2(\omega)\mu'^2[\Lambda_1^2(\omega) + f_e^2(\omega)\Lambda_2^2(\omega)],$$
$$\bar{P}_{22}(\omega, \mu, \mu') = \pi\zeta^2[\Lambda_1^2(\omega) + f_e^2(\omega)\Lambda_2^2(\omega)],$$
$$\bar{P}_{23}(\omega, \mu, \mu') = 0,$$
$$\bar{P}_{24}(\omega, \mu, \mu') = 2\pi f_e(\omega)\zeta^2(\omega)\Lambda_1(\omega)\Lambda_2(\omega)\mu',$$
$$\bar{P}_{31}(\omega, \mu, \mu') = \bar{P}_{32}(\omega, \mu, \mu') = \bar{P}_{33}(\omega, \mu, \mu')$$
$$= \bar{P}_{34}(\omega, \mu, \mu') = 0,$$
$$\bar{P}_{41}(\omega, \mu, \mu') = 2\pi f_e(\omega)\zeta^2(\omega)\Lambda_2(\omega)[\Lambda_1(\omega) + 1]\mu\mu'^2,$$
$$\bar{P}_{42}(\omega, \mu, \mu') = 2\pi f_e(\omega)\zeta^2(\omega)\Lambda_2(\omega)[\Lambda_1(\omega) + 1]\mu,$$
$$\bar{P}_{43}(\omega, \mu, \mu') = 0,$$
$$\bar{P}_{44}(\omega, \mu, \mu') = 2\pi\zeta^2(\omega)[\Lambda_1(\omega) + f_e^2(\omega)\Lambda_2^2(\omega)]\mu\mu'. \tag{2.41}$$

Inserting the results of Eq. (2.41) inside Eqs. (2.36)–(2.39) the explicit expressions of the various source terms can be obtained. The details of this standard manipulation are reported in Appendix B [see, in particular, Eqs. (B1) and (B2)]. The final result is

$$C_I(\omega, \mu) = \frac{1}{4}\{\Delta_{I0}[2\Lambda_3(\omega)(1 - \mu^2)$$
$$+ 2\zeta^2(\omega)(\mu^2 + \Lambda_1^2(\omega)) + 2\zeta^2(\omega)f_e^2(\omega)$$
$$\times \Lambda_1^2(\omega)(1 + \mu^2)] + [2\Lambda_3(\omega)(1 - \mu^2)$$
$$- \zeta^2(\omega)(\mu^2 + \Lambda_1^2(\omega))$$
$$- f_e^2(\omega)\zeta^2(\omega)\Lambda_2^2(\omega)(1 + \mu^2)]S_P$$
$$- 6if_e^2(\omega)\zeta^2(\omega)\Lambda_2(\omega)[\mu^2 + \Lambda_1(\omega)]\Delta_{V1}\}, \tag{2.42}$$

$$C_Q(\omega, \mu) = \frac{1}{4}\{[2(1 - \mu^2)(\Lambda_3(\omega) - \zeta^2(\omega)f_e^2(\omega)\Lambda_2^2(\omega))$$
$$- 2\zeta^2(\omega)(\Lambda_1(\omega) - \mu^2)]\Delta_{I0}$$
$$+ [2\Lambda_3(\omega)(1 - \mu^2) - \zeta^2(\omega)(\mu^2 - \Lambda_1^2(\omega)$$
$$- f_e^2(\omega)\Lambda_2^2(\omega)(1 - \mu^2))]S_P$$
$$- 6if_e^2(\omega)\zeta^2(\omega)\Lambda_2(\omega)(\mu^2 - \Lambda_1(\omega))\Delta_{V1}\}, \tag{2.43}$$

$$C_V(\omega, \mu) = \frac{\zeta^2(\omega)P_1(\mu)}{2}\{f_e(\omega)\Lambda_2(\omega)(\Lambda_1(\omega) + 1)$$
$$\times [2\Delta_{I0} - S_P]$$
$$- \frac{3}{2}i[\Lambda_1(\omega) + f_e^2(\omega)\Lambda_2^2(\omega)]\Delta_{V1}\}, \tag{2.44}$$

while $C_U(\omega, \mu)$ vanishes identically. In Eqs. (2.42)–(2.44) the following important combination has been introduced, namely:

$$S_P = \Delta_{I2} + \Delta_{Q2} + \Delta_{Q0}. \tag{2.45}$$

It must be remarked that S_P is the standard source term arising in the treatment of CMB polarization when the magnetic field contribution is ignored in the scattering process (see, e.g. [33,55,56] and references therein). The result expressed by Eqs. (2.42)–(2.44) does hold to lowest order in the guiding center approximation [see Eq. (A11) and discussion therein]. As it will be discussed in Sec. IV, the results derived so far improve the accuracy of the radiative transfer equations in the case when large-scale magnetic fields are consistently included in the discussion.

The Faraday effect of the CMB is just a rotation of the linear polarization of the CMB and it does not involve the generation of any circular polarization. Faraday effect has been recently treated in greater detail by including various effects which have been neglected in the past [36] (see also [57]). In the case of the Faraday effect, first the linear polarization is generated because of the quadrupole in the intensity of the radiation field and then the polarization is rotated. Also Faraday rotation is treated often in the

uniform field approximation but without the explicit contribution of the magnetic field intensity to the scattering. The present formulation improves also on the treatment of Faraday effect of the CMB (see [10] for an introduction) even if, to keep the discussion self-contained, the focus will be on the generation of the V-mode polarization.

In connection with the Faraday rotation it is appropriate to mention the different physical nature of the approximations often employed in the discussion of large-scale magnetism. In the present paper, as already mentioned, the guiding center approximation has been employed. This approximation (see Appendix A) is particularly sound in the case of scattering problems when the wavelength of the scattered photons is much shorter than the inhomogeneity scale of the magnetic field [51]. The guiding center approximation does not break explicitly the isotropy of the background. As already mentioned in the previous paragraph, Faraday rotation can be discussed in the uniform field approximation [58–61]. The uniform field approximation is independent upon the guiding center approximation: indeed, for instance, in the studies of [58–61] the magnetic field does not contribute to the scattering matrix while it does rotate the polarization plane of the CMB. The uniform field approximation holds provided the magnetic field is not too strong. In the latter case a (new) preferred direction in the sky pops up; a potential correlation of the $a^T_{\ell-1,m}$ and $a^T_{\ell+1,m}$ multipole coefficients is induced and, from this observation, uniform magnetic fields can be constrained [62–65]. This last case is not directly related to the present considerations.

III. CIRCULAR POLARIZATION FROM MAGNETIC KNOTS

It is appropriate to highlight a possible connection between the occurrence of circular polarization and the topological properties of the magnetic flux lines. The occurrence of circular polarization is directly related to the Lorentz force acting either on the individual charge carriers (i.e. $\vec{v}_{e,i} \times \vec{B}$) or on the Ohmic current (i.e. $\vec{J} \times \vec{B}$). In a plasma characterized by a finite conductivity, the presence (or absence) of Lorentz force term can be directly related to the topology of the magnetic flux lines. The topology of the magnetic flux lines can be classified in terms of the so-called magnetic helicity, i.e.

$$\mathcal{N}_B = \int_V d^3x \vec{A} \cdot \vec{B}, \qquad (3.1)$$

where $\vec{A}$ is the vector potential; Eq. (3.1) is the magnetohydrodynamical analog of the kinetic helicity, i.e.

$$\mathcal{N}_\nu = \int d^3x \vec{v} \cdot \vec{\omega}, \qquad \vec{\omega} = \vec{\nabla} \times \vec{v} \qquad (3.2)$$

where $\vec{\omega}$ is the vorticity. In simply connected domains, the magnetic helicity is gauge-invariant provided the normal component of $\vec{B}$ vanishes at the boundary surface of the integration volume V. Furthermore, the helicity is also gauge-invariant if the integration volume is given by a single (or multiple) magnetic flux tube. An important property is that the magnetic helicity is conserved in a highly conducting plasma. In particular, it can be shown, that (see, e.g. [9] or the seminal paper of [47])

$$\frac{d\mathcal{N}_B}{d\tau} = -\frac{1}{4\pi\sigma} \int_V d^3x \vec{B} \cdot \vec{\nabla} \times \vec{B}, \qquad (3.3)$$

where σ is the conductivity. In the limit $\sigma \to \infty$ the magnetic helicity is exactly conserved. In minimizing the total magnetic energy with the constraint that the magnetic helicity be conserved we are naturally led to the variational problem

$$\delta \left[\int_V d^3x(|\vec{B}|^2 - \alpha\vec{A} \cdot \vec{B}) \right] = 0, \qquad (3.4)$$

where α is a Lagrange multiplier. Since $\vec{B} = \vec{\nabla} \times \vec{A}$, the variational problem of Eq. (3.4) is equivalent to

$$\delta \left[\int_V d^3x(|\vec{\nabla} \times \vec{A}|^2 - \alpha\vec{A} \cdot \vec{\nabla} \times \vec{A}) \right] = 0. \qquad (3.5)$$

By making the variation explicit, we have that Eq. (3.5) implies that

$$\vec{\nabla} \times \vec{\nabla} \times \vec{A} = \alpha\vec{\nabla} \times \vec{A}. \qquad (3.6)$$

Going back to the magnetic field we have that the configurations

$$\vec{\nabla} \times \vec{B} = \alpha\vec{B} \qquad (3.7)$$

correspond to the lowest state of magnetic field energy which a closed system may attain. The variational approach leading to the condition (3.7) is due to Woltjer [47] (see also, in this connection [43–46]). The configurations obeying Eq. (3.7) are closely related to the concept of magnetic knot [66] and may arise a consequence of the dynamics of the electroweak phase transition. The presence of pseudoscalar interactions at the electroweak time can twist the magnetic flux lines of the hypermagnetic field and produce a primordial background of hypermagnetic knots [67,68]. It has been speculated that baryogenesis can be related to the presence of hypermagnetic knots and a similar way of thinking has been pursued in [69,70]. The themes discussed in [66,67] stimulated various investigations both on the dynamics of particles in hypermagnetic knot configurations [71–73] as well as on related ideas [74,75].

In solar spectropolarimetry magnetic knots have appeared since the late 1960s [76] (see also, for instance, [77]). An example of magnetic knot configuration is given by:

$$\vec{B}(z) = B_0(\sin kz\hat{x} + \cos kz\hat{y}), \qquad (3.8)$$

satisfying the force-free condition discussed before and

sometimes analyzed in connection with the polarization properties of the synchrotron emission [78,79]. The idea is to distinguish the topology of the magnetic flux lines from the analysis of the circular polarization. In other words: measurements of circular polarization can be used to infer not only the potential existence of large-scale magnetic fields but also their topological structure. As before we are considering here the situation where the ingoing Stokes parameters have no azimuthal dependence. The problem will now be to compute the various entries of the tensor $P_{ij}(\mu, \mu', z)$ which also depend upon the inhomogeneity scale of the knot.

Consider, for simplicity, the case when protons are neglected and only the leading terms are kept in $f_e(\omega)$. In this case we have, quite simply, that the phase matrix, after integration over φ', will be

$$\bar{P}_{11}(\mu, \mu', z) = \pi[2(1 - \mu^2)(1 - \mu'^2) + \mu^2\mu'^2]$$
$$+ \pi f_e(\omega)[3(1 - \mu^2)(1 - \mu'^2) + 1]$$
$$\times \cos[2(kz + \varphi)],$$

$$\bar{P}_{12}(\mu, \mu', z) = \pi\mu^2 + \pi\{1 + \mu^2 \cos[2(kz + \varphi)]\}f_e^2(\omega),$$

$$\bar{P}_{13}(\mu, \mu', z) = 0,$$

$$\bar{P}_{14}(\mu, \mu', z) = 2\pi\mu\mu'\sqrt{1 - \mu^2}f_e(\omega)\sin[kz + \varphi],$$

$$\bar{P}_{21}(\mu, \mu', z) = \pi\mu'^2 + \pi\{1 - \cos[2(kz + \varphi)]\}f_e^2(\omega),$$

$$\bar{P}_{22}(\mu, \mu', z) = \pi + \pi\{1 - \cos[2(kz - \varphi)]\}f_e^2(\omega),$$

$$\bar{P}_{23}(\mu, \mu', z) = 0,$$

$$\bar{P}_{24}(\mu, \mu', z) = 0$$

$$\bar{P}_{31}(\mu, \mu', z) = -2\pi\mu f_e^2(\omega)\sin[2(kz + \varphi)],$$

$$\bar{P}_{32}(\mu, \mu', z) = 0,$$

$$\bar{P}_{33}(\mu, \mu', z) = 0,$$

$$\bar{P}_{34}(\mu, \mu', z) = 2\pi\sqrt{1 - \mu^2}\mu'\cos[kz + \varphi]f_e(\omega),$$

$$\bar{P}_{41}(\mu, \mu', z) = -2\pi\sqrt{1 - \mu^2}(\mu'^2 - 2)f_e(\omega)\sin[kz + \varphi],$$

$$\bar{P}_{42}(\mu, \mu', z) = 2\pi\sqrt{1 - \mu^2}f_e(\omega)\sin[kz + \varphi],$$

$$\bar{P}_{43}(\mu, \mu', z) = 0$$

$$\bar{P}_{44}(\mu, \mu', z) = 2\pi\mu\mu'[1 + f_e^2(\omega)].$$

By integrating over z the relevant matrix elements, i.e.

$$\int_0^{2\pi/k} \bar{P}_{41}(\mu, \mu', z)dz = 0,$$

$$\int_0^{2\pi/k} \bar{P}_{42}(\mu, \mu', z)dz = 0, \qquad (3.9)$$

$$\int_0^{2\pi/k} \bar{P}_{43}(\mu, \mu', z)dz = 0.$$

The same integration, but applied to the linear polariza-

tions, leads to a nonvanishing result. Indeed, the coupling of Δ_I to Δ_Q is controlled by the following matrix element:

$$\bar{P}_{11} + \bar{P}_{12} - \bar{P}_{21} - \bar{P}_{22} = \pi(1 - \mu^2) - 3\pi\mu'^2(1 - \mu^2)$$
$$+ \pi\{3(1 - \mu^2)(1 - \mu'^2)$$
$$+ 2(1 + \mu^2)\cos[2(kz + \varphi)]\}f_e^2$$

$$(3.10)$$

whose integral over z does not vanish and is given by

$$\frac{\pi^2}{k}(1 - \mu^2)(2 - 6\mu'^2) + \frac{2\pi^2}{k}(1 - \mu^2)$$
$$\times [1 + 3\mu'^2 + 2(1 - 3\mu'^2)]f_e^2. \qquad (3.11)$$

The rationale for this occurrence stems from the fact that magnetic knots minimize the magnetic energy subject to the constraint that the helicity is constant. Indeed, over large scales, the minimization of the magnetic energy subjected to the constraint that the magnetic helicity is conserved is equivalent to the condition

$$\vec{\nabla} \times \vec{B} = \frac{\vec{B}}{L} \qquad (3.12)$$

where L is has dimensions of a length and denotes the typical scale of the knot. Over very large scales the displacement current can be neglected and, therefore,

$$\vec{J} = \frac{1}{4\pi}\vec{\nabla} \times \vec{B}, \qquad \vec{J} = en_0(\vec{v}_i - \vec{v}_e). \qquad (3.13)$$

But because of Eq. (3.12) $\vec{J} = \vec{B}/(4\pi L)$ and, therefore, $\vec{J} \times \vec{B} = 0$. This shows that, rather generically, the vanishing of the Lorentz force implies, for these configurations, the vanishing of the circular polarization.

There is another (indirect) way of appreciating this point. It is well known that, at finite conductivity and finite electron density it is possible to construct solutions of the Maxwell equations whose Poynting vector exactly vanishes both in the low-frequency and in the high-frequency limit, i.e. $\vec{E} \times \vec{B} = 0$. These solutions are often dubbed helicity waves since they do not carry momentum but rather helicity [80–82] (see also [83,84]). Consider first helicity waves *in vacuo*. A consistent solution of Maxwell's equations can be written, in this case, as:

$$\vec{E}(z, \tau) = B_0 \frac{k}{\omega}[\sin(kz)\sin(\omega\tau)\hat{x} + \cos(kz)\cos(\omega\tau)\hat{y}],$$

$$\vec{B}(z, \tau) = B_0[\sin(kz)\cos(\omega\tau)\hat{x} + \cos(kz)\cos(\omega\tau)\hat{y}].$$

The above example can also be written as the superposition of circularly polarized waves propagating in opposite directions:

$$\vec{E}(z, \tau) = \frac{kB_0}{2\omega}\{[\cos(kz - \omega\tau) - \cos(kz + \omega\tau)]\hat{x}$$
$$+ [\sin(kz + \omega\tau) - \sin(kz - \omega\tau)]\hat{y}\}. \qquad (3.14)$$

This class of solution can also be obtained at finite electron density and the pertinent dispersion relations are

$$\frac{k^2}{\omega^2} = 1 - \frac{\omega_{pe}^2}{\omega(\omega + i\Gamma)} \qquad (3.15)$$

where Γ is the collision frequency (i.e. the rate of interactions). The Ohm law can be written as:

$$\vec{J} = \frac{e^2 n_e}{m_e} \frac{\vec{E}}{(\Gamma - i\omega)} \simeq \sigma \vec{E}, \qquad \sigma = \frac{\omega_{pe}^2}{4\pi\Gamma}. \qquad (3.16)$$

In the limit $\omega \to 0$ the electric fields are suppressed by the conductivity while the magnetic fields will tend towards the force-free configuration recalled before.

The configuration discussed here has some realistic features and the most relevant drawback is that it is not localized in space. Localized knot configurations can however be constructed (see [68] and references therein and also [85]). It will be interesting to understand the scattering of photons also in these more realistic cases. In spite of that the physical message of the present exercise seems to be that circular polarization of the outgoing radiation is generic provided the underlying magnetic field does affect charged particles. As we saw such an inference is not automatic as long as knotted configurations maximize helicity but minimize the Lorentz force. In the latter case the scattering matrix might not be affected by the magnetic field if the correlation scale of the magnetic knot is much shorter than the Hubble radius at recombination.

IV. ESTIMATES OF THE CIRCULAR POLARIZATION

Building upon the results of Sec. III and taking into account the consideration of Sec. IV it is now appropriate to solve the evolution equations of the brightness perturbations and to obtain explicit estimates of the V-mode power spectra. Since $m_e/m_p \ll 1$ and $f_e(\omega) \ll 1$, Eqs. (2.42)–(2.44) can be safely expanded in powers of (m_e/m_p) as well as in powers of $f_e(\omega)$. The expansion of the scattering matrix in powers of (m_e/m_p) is rather common (already in the absence of any magnetic fields) since, to leading order, the mean free path of the photons is chiefly determined by the scattering on the electrons. The expansion in (m_e/m_p) is common practice in Boltzmann solvers (see, e.g. [86]). In the present case the same strategy will be employed by adding, however, a further expansion parameter, i.e. $f_e(\omega)$.

While the evolution equations of the brightness perturbations for the intensity and for the linear polarization have the first relevant correction going as $f_e^2(\omega)$, the evolution equation for Δ_V has a source term proportional to $f_e(\omega)$. The three functionals appearing in Eqs. (2.42)–(2.44) can then be expanded in powers of (m_e/m_p) and $f_e(\omega)$ with the result that

$$
\begin{aligned}
C_I(\omega, \mu) = &\Delta_{I0}\{1 + [P_2(\mu) + 2]f_e^2(\omega)\} \\
&- \frac{S_P}{2}\{P_2(\mu) + [2 + P_2(\mu)]f_e^2(\omega)\} \\
&- if_e^2(\omega)[2 + P_2(\mu)]\Delta_{V1} + \mathcal{O}\left(\frac{m_e}{m_p}\right) + \mathcal{O}(f_e^4),
\end{aligned}
$$
(4.1)

$$
\begin{aligned}
C_Q(\omega, \mu) = &\frac{1 - P_2(\mu)}{2}\{S_P + f_e^2(\omega)[S_P - 2\Delta_{I0} \\
&+ 2i\Delta_{V1}]\} + \mathcal{O}\left(\frac{m_e}{m_p}\right) + \mathcal{O}(f_e^4),
\end{aligned}
$$
(4.2)

$$
\begin{aligned}
C_V(\omega, \mu) = &\frac{P_1(\mu)}{2}\Big\{2f_e(\omega)[2\Delta_{I0} - S_P] \\
&- \frac{3}{2}i[1 + f_e^2(\omega)]\Delta_{V1}\Big\} + \mathcal{O}\left(\frac{m_e}{m_p}\right) + \mathcal{O}(f_e^4).
\end{aligned}
$$
(4.3)

As anticipated, the source terms for the intensity and for the linear polarization have the first correction going as $f_e^2(\omega)$ while the source term for the circular polarization starts with $f_e(\omega)$. Higher order corrections to Eqs. (4.1)–(4.3) can be computed, if needed recalling the results of Eqs. (2.23)–(2.25) and of Eq. (2.30). Bearing in mind the results of Eqs. (4.1)–(4.3), to lowest order both in (m_e/m_p) and in $f_e(\omega)$ the following system of brightness perturbations can be obtained:

$$
\begin{aligned}
\Delta_I' + n^i \partial_i(\Delta_I + \phi) + \epsilon'\Delta_I \\
= \psi' + \epsilon'\left[\mu v_b + \Delta_{I0} - \frac{P_2(\mu)}{2}S_P\right],
\end{aligned}
$$
(4.4)

$$
\Delta_P' + n^i \partial_i \Delta_P + \epsilon'\Delta_P = \frac{3(1 - \mu^2)\epsilon'}{4}S_P,
$$
(4.5)

$$
\begin{aligned}
\Delta_V' + n^i \partial_i \Delta_V + \epsilon'\Delta_V \\
= \epsilon'P_1(\mu)\Big\{f_e(\omega)[2\Delta_{I0} - S_P] - \frac{3}{4}i\Delta_{V1}\Big\},
\end{aligned}
$$
(4.6)

where all the corrections $\mathcal{O}(f_e^2)$ have been neglected. Note that in Eq. (4.5) Δ_Q has been replaced by Δ_P, i.e. the brightness perturbation for the polarization degree $P = \sqrt{Q^2 + U^2}$. In equivalent terms, as customarily done, we could have chosen the frame where $\Delta_U = 0$. Following the same notation, the source term S_P of Eq. (2.45) will become $S_P = (\Delta_{I2} + \Delta_{P0} + \Delta_{P2})$. If $f_e(\omega) = 0$ in Eq. (4.6) the standard set of brightness perturbations is quickly recovered. In this case the procedure will be to integrate the equations by assuming, for sufficiently early times, that the baryons are tightly coupled with the electrons implying that the baryon velocity is effectively equal to the dipole of the intensity, i.e. $v_b \simeq -3i\Delta_{I1}$. This is, in a nutshell, the

lowest order in the tight-coupling expansion. To lowest order in the tight-coupling expansion the CMB is not polarized in the baryon rest frame, i.e. $\Delta_{I0} \neq 0$ $\Delta_{I1} \neq 0$ but $\Delta_{I2} = \Delta_{P2} = \Delta_{P0} = 0$. To first order in the tight-coupling expansion (linear) polarization is generated and it is proportional, as expected, to the photon quadrupole which can be computed from the lowest order dipole. To summarize the approximations exploited so far we have that

  (i) the scattering matrix has been derived in the guiding center approximation;

  (ii) the brightness perturbations have been then expanded for $f_e(\omega) < 1$;

  (iii) the tight-coupling approximation is not invalidated by the new form of the evolution of the brightness perturbations.

Before giving the details on the line of sight solution of Eqs. (4.4)–(4.6) it is appropriate to pause a moment on the explicit numerical value of $f_e(\omega)$

$$f_e(\omega) = \frac{\omega_{Be}}{\omega} = 2.8 \times 10^{-12}\left(\frac{B_u}{nG}\right)\left(\frac{GHz}{\nu}\right)(z + 1). \quad (4.7)$$

For $z \simeq z_{rec} \simeq 1091$ (see e.g. [22–24]), $f_e(\omega)$ is of the order of 10^{-9} for nG field strengths.[11] In Eq. (4.7) B_u denotes the uniform component of the magnetic field, i.e. we are assuming that the magnetic field is uniform since this is the simplest approximation in which the heat transfer equations can be analyzed. The considerations reported here in the uniform field approximation can be generalized to the case when the magnetic field is characterized by a given power spectrum. As already mentioned at the end of Sec. II the uniform field approximation is more accurate in the present case than in the case of Faraday rotation which will be left for future discussions.

The estimate of Eq. (4.7) can be further reduced by going to higher angular frequencies where, typically, nearly all CMB experiments are operating.[12] Even if $f_e(\omega)$ can be rather small the question remains on the relative magnitude of the VV, VT and BB correlations and this will be one of the points discussed hereunder first for large angular scales (i.e. $\ell < 100$) and then for smaller angular scales when dissipative effects are important.

---

[11]The dependence upon the redshift comes about since the electron and proton masses break the Weyl invariance of the system [see Appendix A and, in particular, Eqs. (A4) and (A5)].

[12]Just to have an idea the Planck explorer satellite is observing the microwave sky in nine frequency channels: three frequency channels (i.e. $\nu = 30, 44, 50$ GHz) belong to the low-frequency instrument; six channels (i.e. $\nu = 100143, 217, 353, 545, 857$ GHz) belong to the high-frequency instrument. The five frequency channels of the WMAP experiment are centered at 23, 33, 41, 61 and 94 in units of GHz. Neither WMAP nor Planck are sensitive to the circular polarizations.

A. Line of sight solutions

Equations (4.4)–(4.6) can be solved, formally, by integration along the line of sight and the result of this step can be written, in Fourier space, as

$$\Delta_I(k, \mu, \tau_0) = \int_0^{\tau_0} e^{-\epsilon(\tau,\tau_0)}(\phi' + \psi')e^{-i\mu x}d\tau$$
$$+ \int_0^{\tau_0} \mathcal{K}(\tau)\left[\Delta_{I0} + \mu v_b - \frac{P_2(\mu)}{2}S_P\right]$$
$$\times e^{-i\mu x}d\tau, \quad (4.8)$$

$$\Delta_P(k, \mu, \tau_0) = \frac{3(1 - \mu^2)}{4}\int_0^{\tau_0} \mathcal{K}(\tau)S_P e^{-i\mu x}d\tau, \quad (4.9)$$

$$\Delta_V(k, \mu, \omega, \tau_0) = \int_0^{\tau_0} \mathcal{K}(\tau)\mu\left\{f_e(\omega)[2\Delta_{I0} - S_P]\right.$$
$$\left. - \frac{3i}{4}\Delta_{V1}\right\}e^{-i\mu x}d\tau, \quad (4.10)$$

where, as usual, $x = k(\tau_0 - \tau)$ and

$$\epsilon(\tau, \tau_0) = \int_\tau^{\tau_0} x_e \tilde{n}_e a d\tau', \qquad \mathcal{K}(\tau) = \epsilon'e^{-\epsilon(\tau,\tau_0)}. \quad (4.11)$$

For large scales the visibility function $\mathcal{K}(\tau)$ can be taken as sharply peaked at the recombination time. For smaller angular scales the (approximately Gaussian) width is essential to obtain sound semianalytical estimates. Recalling the specific form of the lowest order Legendre polynomials [87,88]

$$P_0(\mu) = 1, \qquad P_1(\mu) = \mu, \qquad P_2(\mu) = \frac{1}{2}(3\mu^2 - 1), \quad (4.12)$$

Eqs. (4.4)–(4.6) can be reduced to a hierarchy of coupled evolution equations for the various multipoles. Multiplying Eqs. (4.4)–(4.6) by $P_0(\mu) = 1$ and integrating over μ between -1 and 1, the following relations can be obtained

$$\Delta_{I0}' + k\Delta_{I1} = \psi', \quad (4.13)$$

$$\Delta_{P0}' + k\Delta_{P1} = \frac{\epsilon'}{2}[\Delta_{P2} + \Delta_{I2} - \Delta_{P0}], \quad (4.14)$$

$$\Delta_{V0}' + k\Delta_{V1} = -\epsilon'\Delta_{V0}. \quad (4.15)$$

If Eqs. (4.4)–(4.6) are multiplied by $P_1(\mu)$, both at right- and left-hand sides, the integration over μ of the various terms implies:

$$-\Delta_{I1}' - \frac{2}{3}k\Delta_{I2} + \frac{k}{3}\Delta_{I0} = -\frac{k}{3}\phi + \epsilon'\left[\Delta_{I1} + \frac{1}{3i}v_b\right], \quad (4.16)$$

$$-\Delta'_{P1} - \frac{2}{3}k\Delta_{P2} + \frac{k}{3}\Delta_{P0} = \epsilon'\Delta_{P1}, \qquad (4.17)$$

$$\Delta'_{V1} - \frac{2}{3}k\Delta_{V2} + \frac{k}{3}\Delta_{V0}$$
$$= \epsilon'\left[-\frac{3}{4}\Delta_{V1} + \frac{i}{3}f_e(2\Delta_{I0} - \Delta_{I2} - \Delta_{P2} - \Delta_{P0})\right]. \quad (4.18)$$

The same procedure, using $P_2(\mu)$, leads to:

$$-\Delta'_{I2} - \frac{3}{5}k\Delta_{I3} + \frac{2}{5}k\Delta_{I1} = \epsilon'\left[\frac{9}{10}\Delta_{I2} - \frac{1}{10}(\Delta_{P0} + \Delta_{P2})\right], \qquad (4.19)$$

$$-\Delta'_{P2} - \frac{3}{5}k\Delta_{P3} + \frac{2}{5}k\Delta_{P1} = \epsilon'\left[\frac{9}{10}\Delta_{P2} - \frac{1}{10}(\Delta_{P0} + \Delta_{I2})\right], \qquad (4.20)$$

$$\Delta'_{V2} + \frac{k}{5}[3\Delta_{V2} - 2\Delta_{V1}] = -\epsilon'\Delta_{V2}. \qquad (4.21)$$

For $\ell \geq 3$ the hierarchy of the brightness can be determined in general terms by using the recurrence relation for the Legendre polynomials (see, e.g. [87,88]); the result for $\ell \geq 3$ is

$$\Delta'_{I\ell} + \epsilon'\Delta_{I\ell} = \frac{k}{2\ell+1}[\ell\Delta_{I(\ell-1)} - (\ell+1)\Delta_{I(\ell+1)}],$$
$$\Delta'_{P\ell} + \epsilon'\Delta_{P\ell} = \frac{k}{2\ell+1}[\ell\Delta_{P(\ell-1)} - (\ell+1)\Delta_{P(\ell+1)}],$$
$$\Delta'_{V\ell} + \epsilon'\Delta_{V\ell} = \frac{k}{2\ell+1}[\ell\Delta_{V(\ell-1)} - (\ell+1)\Delta_{V(\ell+1)}].$$
$$(4.22)$$

We are now ready to compute the evolution of the various terms to a given order in the tight-coupling expansion parameter $\tau_c = |1/\epsilon'|$. After expanding the various moments of the brightness and of the baryon velocity in powers of τ_c,

$$\Delta_{I\ell} = \bar{\Delta}_{I\ell} + \tau_c\delta_{I\ell}, \qquad \Delta_{V\ell} = \bar{\Delta}_{V\ell} + \tau_c\delta_{V\ell}, \quad (4.23)$$

$$\Delta_{P\ell} = \bar{\Delta}_{P\ell} + \tau_c\delta_{P\ell}, \qquad v_b = \bar{v}_b + \tau_c\delta_{v_b}, \quad (4.24)$$

the obtained expressions can be inserted into Eqs. (4.13)–(4.18) and the evolution of the various moments of the brightness function can be found order by order in τ_c. To zeroth order in the tight-coupling approximation, $\bar{v}_b = -3i\bar{\Delta}_{I1}$, while Eqs. (4.14)–(4.17) lead, respectively, to

$$\bar{\Delta}_{P0} = \bar{\Delta}_{I2} + \bar{\Delta}_{P2}, \qquad \bar{\Delta}_{P1} = 0, \qquad \bar{\Delta}_{V0} = 0. \quad (4.25)$$

Finally Eqs. (4.19) and (4.20) imply

$$9\bar{\Delta}_{I2} = \bar{\Delta}_{Q0} + \bar{\Delta}_{Q2}, \qquad 9\bar{\Delta}_{Q2} = \bar{\Delta}_{Q0} + \bar{\Delta}_{I2},$$
$$\bar{\Delta}_{V1} = \frac{8}{9}if_e(\omega)\bar{\Delta}_{I0}.$$
$$(4.26)$$

Taking together the four conditions expressed by Eqs. (4.25) and (4.26) we have, to zeroth order in the tight-coupling approximation:

$$\bar{\Delta}_{Q\ell} = 0, \qquad \ell \geq 0, \qquad \bar{\Delta}_{I\ell} = 0, \qquad \ell \geq 2, \quad (4.27)$$

$$\bar{\Delta}_{V\ell} = 0, \qquad \ell \neq 1. \qquad (4.28)$$

Hence, to zeroth order in the tight coupling, the relevant equations are

$$\bar{v}_b = -3i\bar{\Delta}_{I1}, \qquad (4.29)$$

$$\bar{\Delta}'_{I0} + k\bar{\Delta}_{I1} = \psi', \qquad (4.30)$$

$$\bar{\Delta}_{V1} = \frac{8}{9}if_e(\omega)\bar{\Delta}_{I0}. \qquad (4.31)$$

Even if to zeroth order in the tight-coupling expansion we have that the linear polarization is absent. To get a nonvanishing linear polarization we have to go to first order where the monopole and the dipole of the linear polarization are proportional to the quadrupole of the intensity; at the same order in the perturbative expansion the nonvanishing quadrupole of the circular polarization is also generated. Indeed, recalling Eqs. (4.23) and (4.24), the first-order results can be written as

$$\delta_{Q0} = \frac{5}{4}\delta_{I2}, \qquad \delta_{Q2} = \frac{1}{4}\delta_{I2}, \qquad (4.32)$$

$$\delta_{I2} = \frac{8}{15}k\bar{\Delta}_{I1}, \qquad \delta_{V2} = \frac{2}{5}k\bar{\Delta}_{V1}. \qquad (4.33)$$

From Eqs. (4.32) and (4.33) the line of sight solution of Eq. (4.10) can be written as

$$\Delta(k, \mu, \omega, \tau_0) = \int_0^{\tau_0} \mathcal{K}(\tau)\mu\left\{\frac{8}{3}f_e(\omega)\bar{\Delta}_{I0}(k, \tau)\right.$$
$$\left. - \frac{f_e(\omega)}{3}(k\tau_c)\bar{\Delta}_{I1}\right\}e^{-i\mu x}d\tau, \qquad (4.34)$$

where Eqs. (4.29) and (4.30) have also been used. The result of Eq. (4.34) has been used in [89] and the present discussion corroborates and extends those results.

In the sudden decoupling approximation the visibility function becomes effectively a Dirac delta function and the second term (proportional to the dipole of the intensity) can be neglected in comparison with the monopole whose evolution equation can be written as

$$\bar{\Delta}''_{I0} + \frac{\mathcal{H}R_b}{R_b+1}\bar{\Delta}'_{I0} + \frac{k^2}{3(R_b+1)}\bar{\Delta}_{I0} = \Sigma_\psi + \Sigma_B, \quad (4.35)$$

where $R_b = (3/4)\rho_b/\rho_\gamma$ is the baryon to photon ratio and where

$$\Sigma_\psi = \psi'' + \frac{\mathcal{H}R_b}{R_b+1}\psi' - \frac{k^2}{3}\phi \qquad (4.36)$$

$$\Sigma_B = \frac{k^2}{12(R_b + 1)}(4\sigma_B - \Omega_B). \tag{4.37}$$

Equation (4.37) accounts for the presence of an inhomogeneous magnetic field (see [34,90,91] for a definition) but in the estimates we are going to present here, the inhomogeneities stemming from the magnetic field itself will be neglected for consistency with the uniform field approximation.

It is finally appropriate to remark that it is possible to go improve on the accuracy of the line of sight solutions for the V-mode polarization. For this purpose the technique developed in Ref. [56] will be extended to the line of sight solution of the V-mode polarization. To be specific consider, again, the system of Eqs. (4.8), (4.9), and (4.10). In particular we shall be interested in improving on Eq. (4.34) which has been derived from Eq. (4.10). Instead of using the lowest order tight-coupling solution for the linear polarization source it is possible to resum the perturbative expansion by solving an effective evolution equation for S_P. Recall, for this purpose, that the conformal time derivative of S_P, i.e. $S_P' = (\Delta_{I2}' + \Delta_{P0}' + \Delta_{P2}')$ can be expressed as the sum of the evolution equations of the separate multipoles. In particular Δ_{P0}' can be expressed from Eq. (4.14), Δ_{I2}' can be expressed from Eq. (4.19) and Δ_{P2}' from Eq. (4.20). Summing up the various contributions and rearranging the relevant terms an effective evolution equation for S_P can be obtained and it is

$$S_P' + \frac{3}{10}\epsilon' S_P = k\left[\frac{2}{5}\Delta_{I1} - \frac{3}{5}(\Delta_{P1} + \Delta_{P3} + \Delta_{I3})\right], \tag{4.38}$$

which can be solved in different ways. For instance, if only the intensity dipole is kept, at the right-hand side of Eq. (4.38) the result for S_P is

$$S_P(k, \tau) = \frac{2}{5}ke^{3\epsilon(\tau,\tau_0)/10}\int_0^\tau d\tau' \bar{\Delta}_{I1}(k, \tau')e^{-3\epsilon(\tau',\tau_0)/10}. \tag{4.39}$$

If we now insert Eq. (4.39) into Eq. (4.10) the integrals can be performed, up to some point, with analytic techniques. This result improves then Eq. (4.34).

The considerations developed so far suggest the following physical picture. To lowest order in the tight-coupling expansion the presence of a magnetic field produces a dipole of the circular polarization. The dipole of the V mode can be fed back into the line of sight solution to obtain the higher multipoles in full analogy with what is customarily done in Boltzmann solvers. While the circular polarization is building up from the monopole of the intensity, the dipole of the intensity sources, to first- order in the tight-coupling expansion, the linear polarization and, in particular, Δ_{P0} and Δ_{P1}. The interesting aspect of this analysis is that, indeed, to lowest order in the tight-coupling approximation the CMB is circularly polarized

if a predecoupling magnetic field is present. The linear polarization is generated to first order in the tight-coupling expansion. At the level of the amplitude, as it will be shown, the angular power spectrum of the V mode is always smaller than the E-mode spectrum which arises directly from Δ_P. The reason for this occurrence stems from the specific value of $f_e(\omega)$.

B. Large-scale limit

For large angular scales the circular polarization will then be given by

$$\Delta_V(k, \mu, \tau_0) = \frac{8}{3}\int_0^{\tau_0} \mathcal{K}(\tau)f_e(\omega)e^{-i\mu k(\tau_0-\tau)}\mu\bar{\Delta}_{I0}(k, \tau)d\tau, \tag{4.40}$$

where $\bar{\Delta}_{I0}$ can be determined from Eqs. (4.29), (4.30), (4.31), and (4.35). The terms arising in S_P have been neglected since they vanish to lowest order in the tight-coupling expansion. By assuming that $\mathcal{K}(\tau)$ is a Dirac delta function centered at recombination (sudden decoupling approximation) we shall have that

$$\Delta_V(k, \mu, \tau_0, \omega) = \frac{8}{3}f_e(\omega)e^{-i\mu x}\mu\bar{\Delta}_{I0}(k, \tau_{\rm rec}). \tag{4.41}$$

Let us now compute the angular power spectrum of the circular polarization.

$$\Delta_V(\hat{n}, \tau_0) = \sum_{\ell,m}a_{\ell m}^{(V)}Y_{\ell m}(\hat{n}), \tag{4.42}$$

thus we will also have that

$$a_{\ell m}^{(V)} = \int d\hat{n}\Delta_V(\hat{n}, \tau_0)Y_{\ell m}^*(\hat{n})$$

$$= \frac{1}{(2\pi)^{3/2}}\int d\hat{n}\int d^3k\Delta_V(k, \mu, \tau_0)Y_{\ell m}^*(\hat{n}). \tag{4.43}$$

Recalling the explicit expression of $\Delta_V(k, \mu, \tau_0)$

$$a_{\ell m}^{(V)} = \frac{8f_e(\omega)}{3(2\pi)^{3/2}}\int d\hat{n}\int d^3kY_{\ell m}^*(\hat{n})\mu e^{-i\mu x}\Delta_{I0}(k, \tau_{\rm rec})$$

$$= \frac{8if_e(\omega)}{3(2\pi)^{3/2}}\int d\hat{n}\int d^3kY_{\ell m}^*(\hat{n})\frac{d}{dx}(e^{-i\mu x})\Delta_{I0}(k, \tau_{\rm rec}). \tag{4.44}$$

The integration over $d\hat{n} = \sin\vartheta d\varphi d\vartheta = -d\mu d\varphi$ can be performed in explicit terms since $e^{-i\mu x}$ can be expanded in Rayleigh series and the final result is

$$a_{\ell m}^{(V)} = -\frac{8}{3}\delta_{m0}\frac{(-i)^{\ell+1}}{(2\pi)^{3/2}}f_e\sqrt{4\pi}\sqrt{2\ell + 1}$$

$$\times \int d^3k\left(\frac{dj_\ell}{dx}\right)\Delta_{I0}(k, \tau_{\rm rec}). \tag{4.45}$$

The angular power spectrum of the circular polarization can then be written as

$$C_\ell^{(VV)}(\omega) = \frac{1}{2\ell + 1} \sum_{m=-\ell}^{\ell} \langle a_{\ell m}^{(V)*} a_{\ell m}^{(V)} \rangle$$

$$= \frac{256\pi}{9} f_e^2(\omega) \int_0^\infty \frac{dk}{k} \frac{k^3}{2\pi^2} \left(\frac{dj_\ell}{dx}\right)^2 |\Delta_{I0}(k, \tau_{\rm rec})|^2,$$

(4.46)

where the dependence on the angular frequency ω has been explicitly included in the expression of the angular power spectrum. The large-scale estimate of $\bar\Delta_{I0}(k, \tau_{\rm rec})$ follows from Eq. (4.13) by neglecting the dipole which is negligible for those wavelengths which are still larger than the Hubble radius around the redshift of recombination:

$$\bar\Delta_{I0}(k, \tau_{\rm rec}) = \bar\Delta_{I0}(k, \tau_*) + \psi(k, \tau_{\rm rec}) - \psi_*(k), \quad (4.47)$$

where, by definition, $\psi(k, \tau_*) = \psi_*(k)$ and $\phi(k, \tau_*) = \phi_*(k)$ are the values of the metric fluctuations at $\tau_* \ll \tau_{\rm eq}$. For $\tau \simeq \tau_*$ $k\tau_* \ll 1$ and, in the minimal ΛCDM scenario, the initial conditions are (predominantly) adiabatic, i.e.

$$\delta_\gamma(k, \tau_*) = -2\phi_*(k), \qquad \psi(k, \tau_*) = \psi_*(k)$$

$$\mathcal{R}_*(k) = -\psi_*(k) - \frac{\phi_*(k)}{2},$$

(4.48)

implying

$$\Delta_{I0}(k, \tau_{\rm rec}) = \frac{2(R_\nu + 15)}{5(4R_\nu + 15)} \mathcal{R}_*(k),$$

$$\psi_*(k) = \left(1 + \frac{2}{5}R_\nu\right)\phi_*(k),$$

(4.49)

where R_ν is the fractional contribution of the massless

neutrinos to the radiation background.[13] The angular power spectrum is

$$C_\ell^{(VV)}(\omega) = \frac{512\pi^2}{225}\left(\frac{R_\nu + 15}{4R_\nu + 15}\right)^2 f_e^2(\omega) \mathcal{A}_\mathcal{R}\left(\frac{k_0}{k_p}\right)^{n_s - 1}$$

$$\times \mathcal{I}^{(VV)}(\ell, n_s),$$

$$\mathcal{I}^{(VV)}(\ell, n_s) = \frac{2\ell(\ell + 1)}{\pi} \int_0^\infty dx x^{n_s - 2}\left(\frac{dj_\ell}{dx}\right)^2.$$

The derivative of the spherical Bessel function can be expressed in terms of the appropriate recurrence relations, namely [87,88]:

$$\frac{dj_\ell}{dx} = \frac{\ell}{x} j_\ell(x) - j_{\ell+1}(x). \quad (4.50)$$

The integral becomes then:

$$\mathcal{I}^{(VV)}(\ell, n_s) = \ell(\ell + 1) \int_0^\infty dx x^{n_s - 5}[\ell^2 J_{\ell+1/2}^2(x)$$

$$+ x^2 J_{\ell+3/2}^2(x) - 2\ell x J_{\ell+1/2}(x) J_{\ell+3/2}(x)],$$

(4.51)

which can be explicitly computed [87,88]. The final result for the angular power spectrum can therefore be written as

$$\frac{\ell(\ell + 1)}{2\pi} C_\ell^{(VV)}(\omega) = \frac{256\pi}{225}\left(\frac{R_\nu + 15}{4R_\nu + 15}\right)^2 f_e^2(\omega)$$

$$\times \mathcal{A}_\mathcal{R}\left(\frac{k_0}{k_p}\right)^{n_s - 1} \mathcal{I}^{(VV)}(\ell, n_s), \quad (4.52)$$

where

$$\mathcal{I}_\ell^{(VV)}(n_s) = \frac{\ell(\ell + 1)[4\ell(\ell + 1) - (n_s - 1)(n_s - 2)(n_s - 4)]\Gamma(3 - n_s)\Gamma(\ell - 3/2 + n_s/2)}{2^{6 - n_s}\Gamma(2 - n_s/2)\Gamma(3 - n_s/2)\Gamma(\frac{7}{2} + \ell - n_s/2)}. \quad (4.53)$$

Following the same technique we can estimate the cross correlation between temperature and polarization as:

$$\frac{\ell(\ell + 1)}{2\pi} C_\ell^{(VT)}(\omega) = \frac{16\pi}{75} f_e(\omega) \frac{(R_\nu + 15)(2R_\nu - 15)}{(4R_\nu + 15)^2}\left(\frac{k_0}{k_p}\right)^{n_s - 1} \mathcal{I}^{(VT)}(\ell, n_s), \quad (4.54)$$

where

$$\mathcal{I}^{(VT)}(\ell, n_s) = \ell(\ell + 1) \int_0^\infty dx x^{n_s - 4}[\ell J_{\ell+1/2}^2(x) - x J_{\ell+1/2}(x) J_{\ell+3/2}(x)]. \quad (4.55)$$

By integrating the above expression we have that:

$$\mathcal{I}^{(VT)}(\ell, n_s) = \frac{\ell(\ell + 1)(2 - n_s)\Gamma(2 - n_s/2)\Gamma(\ell + n_s/2 - 1)}{4\sqrt{\pi}\Gamma(5/2 - n_s/2)\Gamma(\ell - n_s/2 + 3)}. \quad (4.56)$$

---

[13]Neutrinos are taken to be massless for consistency with ΛCDM paradigm even if the effect of the masses could be included without appreciable changes in the forthcoming numerical estimates.
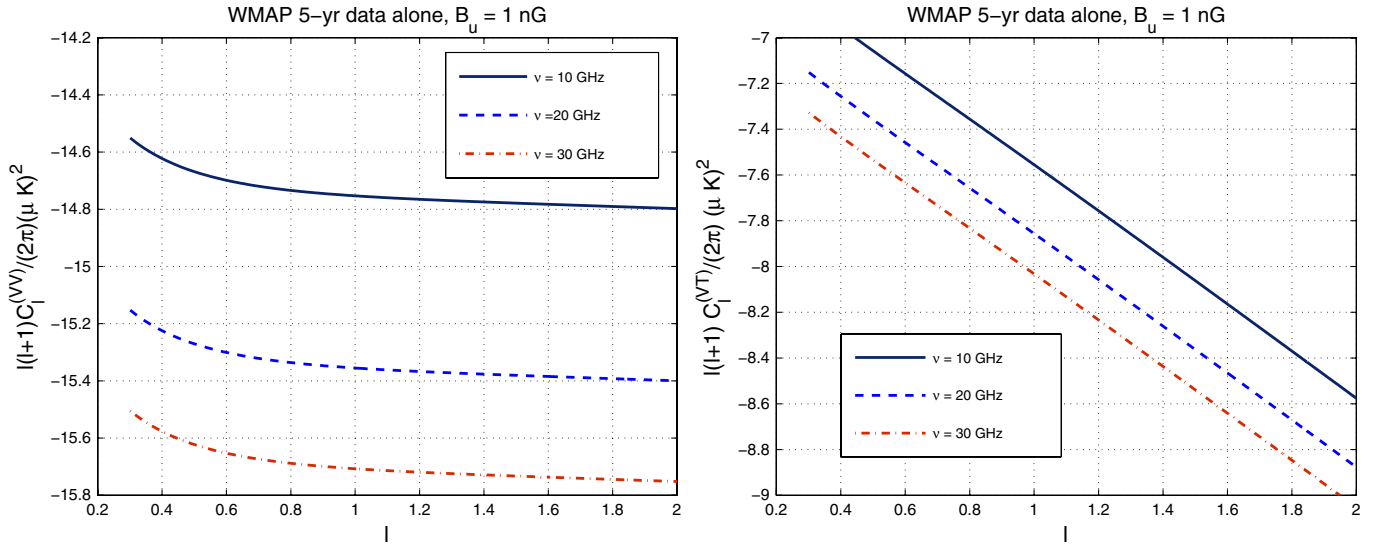
FIG. 1 (color online).   The *VV* and *VT* angular power spectra are illustrated for large angular scales and for different frequencies at a fixed value of the magnetic field intensity. In both plots a double logarithmic scale has been employed, i.e. on both axes we plot the common logarithms of the corresponding quantity.

In Fig. 1 the *VV* and the *VT* angular power spectra are illustrated for large angular scales (i.e. $\ell < 100$). Both in Fig. 1 and in Fig. 2 a double logarithmic scale has been used. In Fig. 1 the uniform magnetic field intensity is fixed while the frequency ranges between 10 and 30 GHz. Note that 30 GHz corresponds to the lower frequency band of the Planck explorer satellite which is unfortunately not sensitive to the circular polarization. In Fig. 1 the cosmological parameters have been fixed as

$$(\Omega_b, \Omega_c, \Omega_{de}, h_0, n_s, \epsilon_{re}) \equiv (0.0441, 0.214, 0.742,$$
$$0.719, 0.963, 0.087), \qquad (4.57)$$

corresponding to the best fit of the WMAP data alone in the light of the vanilla ΛCDM. In Fig. 2 the frequency is fixed to 10 GHz while the magnetic field intensity changes from 1 to 10 nG. The values of the magnetic field intensity are motivated by a recent analysis [34] where using the *TE* and *TT* correlations the parameters of a putative magnetized background are scrutinized. According to [33,34] nG magnetic fields and blue magnetic spectral indices are fully compatible with the measured values of the *TT* and *TE* angular power spectra.

The results of Fig. 1 and of Fig. 2 show already that the values of the *VT* correlations are close to the magnitude of
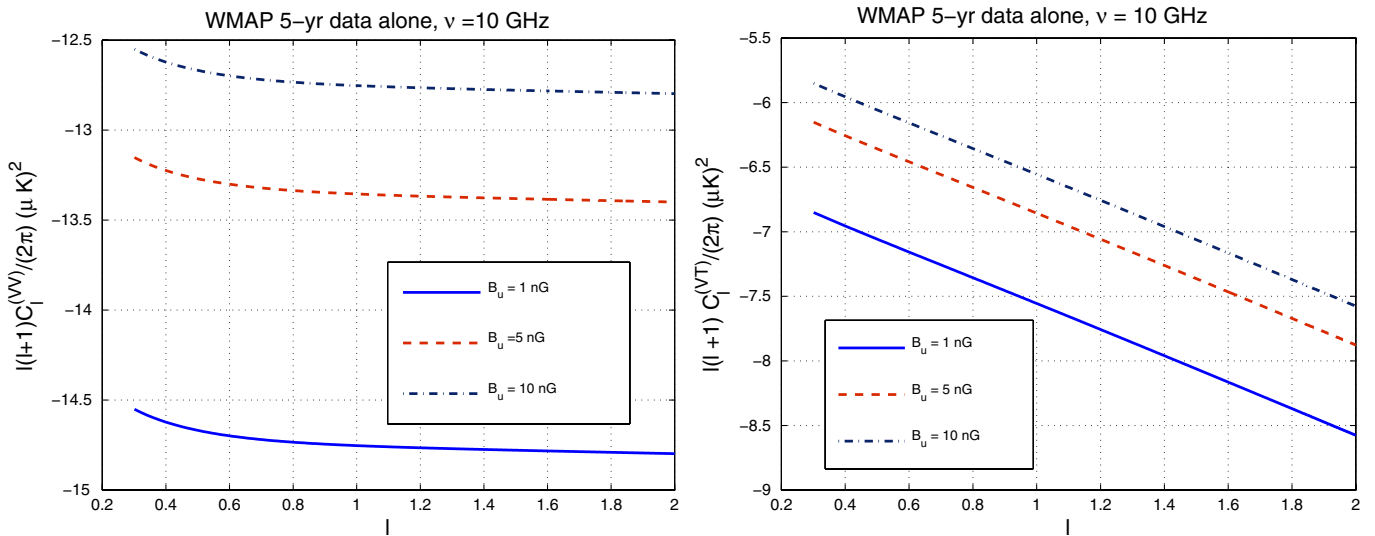

FIG. 2 (color online).   The *VV* and *VT* angular power spectra are illustrated for large angular scales and for different values of the magnetic field intensity at a fixed value of the frequency. As in Fig. 1 a double logarithmic scale has been employed in both plots of the present figure.

the BB angular power spectra from gravitational lensing as well as to the BB angular power spectra expected from the tensor modes of the geometry. It is important to remind the reader here that the VV and VT angular power spectra are a direct consequence of, both, the weakly magnetized plasma and the adiabatic mode of curvature perturbations. Absent one of these two essential ingredients the net result would vanish. The considerations reported so far complement some of the results already reported in [89]. The large-scale (analytical) estimates will now be corroborated by the numerical results at smaller angular scales.

C. Small-scale limit

The visibility function vanishes for $\tau \gg \tau_{\rm rec}$ and has a maximum around recombination, i.e. when

$$\epsilon'' + \epsilon'^2 = 0, \qquad \frac{d\epsilon}{d\tau} = -x_e(\tau)\tilde{n}_e(\tau)\sigma_{\rm Th}a(\tau) \equiv -\epsilon'. \tag{4.58}$$

The second expression in Eq. (4.58) clarifies that a minus sign appears in the time derivative of $\epsilon(\tau, \tau_0)$ since τ appears in the lower limit of integration. When the finite thickness effects of the last scattering surface are taken into account the visibility function can be approximated by a Gaussian profile centered at $\tau_{\rm rec}$, i.e.

$$\mathcal{K}(\tau) = \mathcal{N}(\sigma_{\rm rec})e^{-(\tau-\tau_{\rm rec})^2/(2\sigma_{\rm rec}^2)},$$
$$\int_0^{\tau_0} \mathcal{K}(\tau)d\tau = 1, \tag{4.59}$$

$$\mathcal{N}(\sigma_{\rm rec}) = \sqrt{\frac{2}{\pi}}\frac{1}{\sigma_{\rm rec}}\left[\text{erf}\left(\frac{\tau_0-\tau_{\rm rec}}{\sqrt{2}\sigma_{\rm rec}}\right) + \text{erf}\left(\frac{\tau_{\rm rec}}{\sqrt{2}\sigma_{\rm rec}}\right)\right]^{-1}, \tag{4.60}$$

$$\text{erf}(z) = \frac{2}{\sqrt{\pi}}\int_0^z e^{-t^2}dt. \tag{4.61}$$

The overall normalization $\mathcal{N}(\sigma_{\rm rec})$ has been chosen in such a way that the integral of $\mathcal{K}(\tau)$ is normalized to 1:

the visibility function is nothing but the probability that a photon last scatters between τ and $\tau + d\tau$. Equation (4.60) simplifies when $\tau_0 \gg \tau_{\rm rec}$ and $\tau_0 \gg \sigma_{\rm rec}$, since, in this limit, the error functions go to a constant and $\mathcal{N}(\sigma_{\rm rec}) \to \sigma_{\rm rec}^{-1}\sqrt{2/\pi}$. In the latter limit, the thickness of the last scattering surface, i.e. $\sigma_{\rm rec}$, is of the order of $\tau_{\rm rec}$. The Gaussian approximation for the visibility function has a long history (see, e.g. [92–95]). The WMAP data suggest a thickness (in redshift space) $\Delta z_{\rm rec} \simeq 195 \pm 2$ which would imply that $\sigma_{\rm rec}$, in units of the (comoving) angular diameter distance to recombination, can be estimated as $\sigma_{\rm rec}/\tau_0 \simeq 1.43 \times 10^{-3}$. By using the finite width of the visibility function we have that

$$a_{\ell m}^{(V)} = -\delta_{m0}\frac{8(-i)^{\ell+1}}{3(2\pi)^{3/2}}f_e\sqrt{4\pi}\sqrt{2\ell+1}\int d^3k\left(\frac{dj_\ell}{dx}\right)$$
$$\times e^{-k^2/k_t^2}\mu\bar{\Delta}_{I0}(k, \tau_{\rm rec})e^{-\epsilon_{\rm re}}, \tag{4.62}$$

where $k_t = (\sqrt{6}/\sigma_{\rm rec})$, $x = k(\tau_0 - \tau_{\rm rec})$. The visibility function, more realistically, also has a second peak at the reionization epoch (i.e. for $z_{\rm re} = 11 \pm 1.4$). Also in this case the visibility function can be approximated with a Gaussian profile centered, this time, around $\tau_{\rm re}$ and this consideration introduces a suppression going as $e^{-\epsilon_{\rm re}}$. In the limit $\tau_0 \gg \tau_{\rm rec}$ and $\tau_0 \gg \sigma_{\rm rec}$ the integral to be computed is, therefore,

$$\frac{\ell(\ell+1)}{2\pi}C_\ell^{(VV)}(\omega) = 8f_e^2(\omega)\int_0^\infty e^{-2(k^2/k_t^2)}\frac{k^3}{2\pi^2}$$
$$\times |\Delta_{I0}(k, \tau_{\rm rec})|^2(\ell+1)\ell\left(\frac{dj_\ell}{dx}\right)^2. \tag{4.63}$$

Recalling that

$$\left(\frac{dj_\ell}{dx}\right)^2 = \left[1 - \frac{\ell(\ell+1)}{x^2}\right]j_\ell^2(x) + \frac{1}{2x}\frac{d^2}{dx^2}[xj_\ell^2(x)] \tag{4.64}$$

the Bessel functions can be estimated in the limit of very large multipoles. A standard calculation then leads to

$$\frac{\ell(\ell+1)}{2\pi}C_\ell^{(VV)} = \frac{32}{9}f_e^2(\omega)\mathcal{A}_\mathcal{R}\left(\frac{k_0}{k_p}\right)^{n_s-1}\ell^{n_s-1}\int_1^\infty w^{n_s-5}\sqrt{w^2-1}dw[(2L_\mathcal{R}^2(w, \ell)e^{-2(\ell/\ell_t)^2w^2} + M_\mathcal{R}^2(w, \ell)c_{\rm sb}e^{-2(\ell/\ell_s)^2w^2})$$
$$+ M_\mathcal{R}^2(w, \ell)c_{\rm sb}\cos[2(\gamma_A w\ell)]e^{-2(\ell/\ell_s)^2w^2} + 4L_\mathcal{R}(w, \ell)M_\mathcal{R}(w, \ell)\sqrt{c_{\rm sb}}\cos(\gamma_A w\ell)e^{-[(\ell/\ell_s)^2+(\ell/\ell_t)^2]w^2}], \tag{4.65}$$

where $c_{\rm sb} = [3(R_b + 1)]^{-1/2}$ is the baryon sound speed. Following Ref. [34] we introduced in Eq. (4.65) the quantities[14]

---

[14]It is understood that all the quantities are computed for at $z = z_{\rm rec}$; furthermore $r_R = \rho_R/\rho_M = 4.15 \times 10^{-2}\omega_M(z/1000)$.
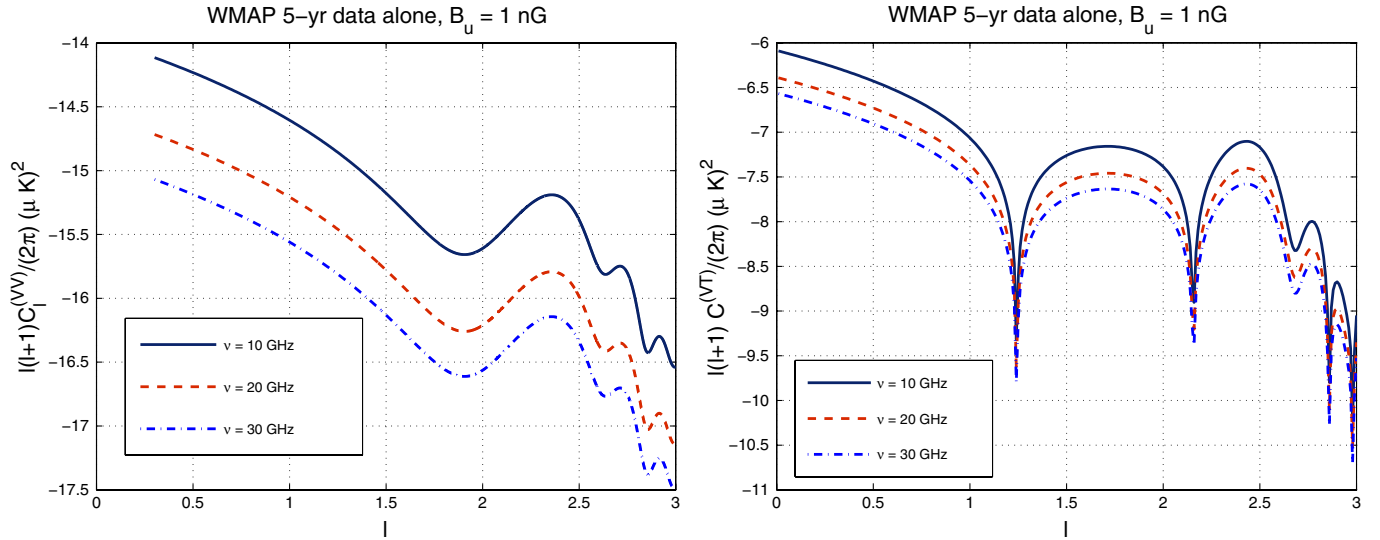
FIG. 3 (color online).   The VV and VT angular power spectra are illustrated for small angular scales and for different values of the frequency and for fixed magnetic field intensity. As in Fig. 2 a double logarithmic scale has been employed in both plots.

$$L_{\mathcal{R}}(w, \ell) = \alpha_{\mathcal{R}} - \beta_{\mathcal{R}} \ln[wq_\ell],$$

$$M_{\mathcal{R}}(w, \ell) = \bar{\alpha}_{\mathcal{R}} + \bar{\beta}_{\mathcal{R}} \ln[wq_\ell],$$

$$q_\ell = \left(\frac{\ell}{200 d_A(z)}\right)\sqrt{\frac{r_R}{z+1}}, \qquad \alpha_{\mathcal{R}} = \frac{R_b + 1}{6},$$

$$\beta_{\mathcal{R}} = \frac{R_b}{6}, \qquad \bar{\alpha}_{\mathcal{R}} = -\frac{6}{25}\ln(96),$$

$$\bar{\beta}_{\mathcal{R}} = -\frac{6}{25}. \tag{4.66}$$

In Eq. (4.66) the quantity $d_A(z)$ is related to the angular diameter distance $D_A(z)$ as $d_A(z) = \sqrt{\Omega_{M0}} H_0 D_A(z)/2$. Furthermore γ_A and ℓ_D can be estimated as follows[15]

$$\gamma_A = \frac{d_A^{-1}(z)}{\sqrt{3R_b(z+1)}} \ln\left[\frac{\sqrt{1 + R_b} + \sqrt{R_b}\sqrt{1 + r_R}}{1 + \sqrt{r_R R_b}}\right],$$

$$\ell_D = k_D D_A(z) = \frac{2240 d_A(z_*)}{\sqrt{\sqrt{r_R + 1} - \sqrt{r_R}}}\left(\frac{z}{10^3}\right)^{5/4} \omega_b^{0.24} \omega_M^{-0.11}. \tag{4.67}$$

The Silk multipole is just expressed in terms of ℓ_t and ℓ_D as $\ell_S = \ell_t \ell_D / \sqrt{\ell_t^2 + \ell_D^2}$. With the same approach it is possible to express, for small angular scales, the cross correlation $C_\ell^{(VT)}(\omega)$.

For more reliable estimates at small scales fully numerical methods should be employed and the results, consistent with the previous analytic estimates, are illustrated in Figs. 3 and 4. In Fig. 3 the VV and VT angular power spectra are illustrated on a double logarithmic scale. The spikes appearing in the VT correlation are the usual feature

_____

[15]Following the usual convention we shall denote $\omega_X = h_0^2 \Omega_{X0}$ for a generic species.

displayed when plotting the modulus of the cross correlation. The same spikes occur when plotting the logarithm of the modulus of the TE power spectrum. In Fig. 3 the magnetic field is fixed to 1 nG while the frequency of the channel is allowed to vary. In Fig. 4 the VV and VT correlations are illustrated for a fixed value of the frequency but for various magnetic field intensities.

The moment has now come to compare the signal from circular dichroism with the signals expected from the linear polarization. The spirit of the forthcoming considerations is just to compare the orders of magnitude of the different contributions. While this step is mandatory within the present analysis it is also not conclusive, from the experimental point of view. Indeed different signals and different correlation functions inherit from nature different systematic effects. The latter problem is of course extremely important and will not be treated here.

Let us first of all compare the V-mode signal with the measurements (and expectations) of the ΛCDM paradigm. A simple comparison is illustrated in Table I where the different angular power spectra are reported at the peak. The TT power spectrum at the first acoustic peak is of the order of 6000 $(\mu K)^2$. The TE and the EE angular power spectra peak for larger multipoles. The WMAP team measured with reasonable accuracy the region of the first anticorrelation peak of the TE power spectrum and the lowest multipoles of the EE power spectrum. The recent QUaD measurements gave a rather interesting evidence of the oscillations in the EE angular power spectra at larger ℓ. The absolute value of the TE angular power spectrum peaks around $\ell \sim 750$ and it is of the order of 130 $(\mu K)^2$. The EE correlation reaches a value of 40 $(\mu K)^2$ for $\ell \sim 1000$. The quoted figures are consistent with the expectations of the ΛCDM scenario with no tensors (also sometimes called vanilla ΛCDM). In the
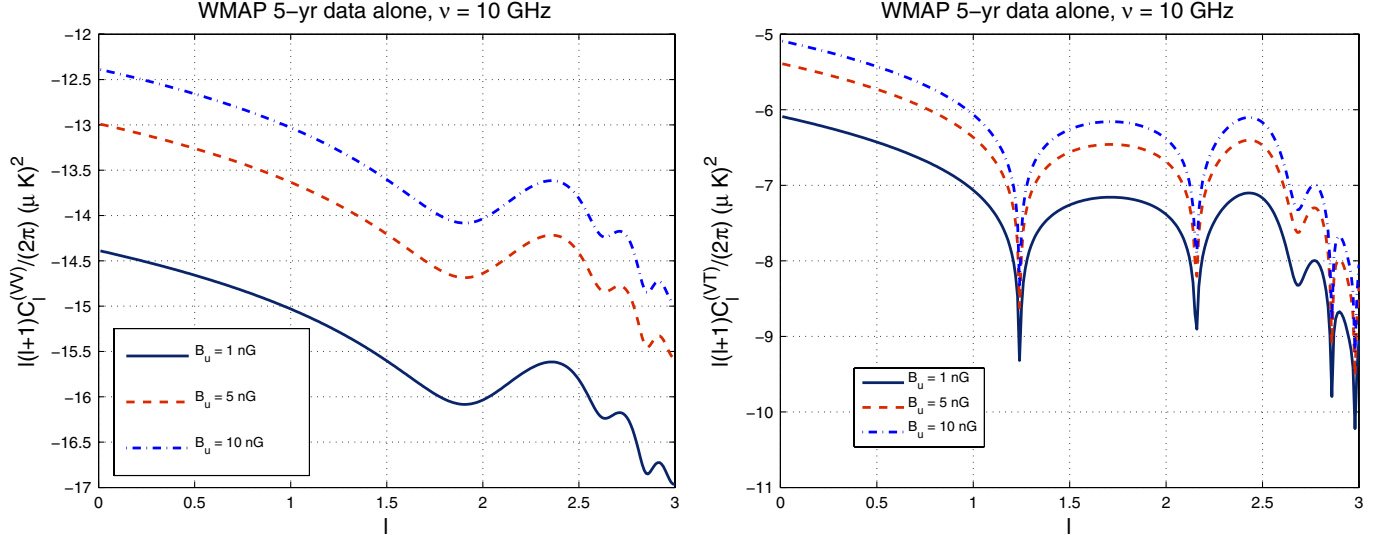
FIG. 4 (color online).   The VV and VT angular power spectra are illustrated for small angular scales and for different values of the magnetic field at a fixed value of the frequency. As in the previous figures, a double logarithmic scale has been employed.

TABLE I.   The values of the different angular power spectra at the peak (illustrative figures for $B_u = 1$ nG and $\nu = 10$ GHz).

Data	$\ell_{\rm peak}$	$\ell_{\rm peak}(\ell_{\rm peak} + 1)C^{(XX)}_{\ell_{\rm peak}}/(2\pi)$
TT	220	5756 $(\mu{\rm K})^2$
EE	1000	40 $(\mu{\rm K})^2$
TE	750	130 $(\mu{\rm K})^2$
VT	$\ell < 50$	10^{-6} $(\mu{\rm K})^2$
VV	$\ell < 50$	10^{-14} $(\mu{\rm K})^2$

vanilla ΛCDM the only potential source of B-mode polarization is represented by gravitational lensing of the primary anisotropies. The typical values of the induced BB angular power spectrum range between 10^{-8} $(\mu{\rm K})^2$ and 10^{-5} for $\ell < 50$. In Table I the expectations for the VV and VT angular power spectra are reported in the case of a hypothetical low frequency instrument sensitive to V-mode polarization operating in a band with central frequency of the order of 10 GHz. The intensity of the (comoving) magnetic field has been taken to be 1 nG. As previously discussed both analytically and numerically the VV and VT power spectra are larger for low multipoles. For larger multipoles, however, the effects of the thickness of the visibility function and of the diffusive damping come into play only for $\ell \sim 1000$. In this sense the range of multipoles highlighted in Table I should be complemented with the results illustrated in Figs. 1–4.

The comparison summarized in Table I does not contemplate the BB angular power spectrum stemming from the tensor modes of the geometry which is regarded as the main target of running experiments such as Planck. The B-mode power spectrum induced by relic gravitons peaks for $\ell \sim 90$ corresponding to an angular scale of roughly

2 deg. The signal, however, depends upon r_T (i.e. the ratio between the tensor and the scalar power spectrum) for which only upper limits exist. Depending upon the data sets chosen for the analysis the putative limit on r_T slightly changes. The situation is quickly summarized in Table II where the upper limits on r_T are reported at the pivot scale $k_p = 0.002$ Mpc^{-1} and in the case where the scalar spectral index does not run. Slightly larger values of r_T are allowed if n_s is allowed to run but this aspect will not be essential for the present considerations.[16] The comparison between the VV and VT power spectra and the other polarization power spectra is also illustrated, more visually, in Fig. 5. In the plot at the left of Fig. 5 the upper curve corresponds, as indicated by the legend, to the EE angular power spectra obtained from the best fit to the WMAP 5-yr data alone [see Eq. (4.57)]. In the plot at the right the B-mode polarization is illustrated when a tensor mode contribution is allowed.

It is tempting to speculate, at this point, that, indeed, low frequency instruments could make the difference for scrutinizing a potential V-mode polarization. In this respect the results and the techniques of [40–42] (as well as the earlier results of [38,39]) could be probably revisited in the light of the considerations developed here. It has been shown that the VT correlation for a comoving magnetic field from 5 to 10 nG can be as large as 10^{-5} $(\mu{\rm K})^2$ at 10 GHz for $\ell < 20$ (i.e. large angular separations). This means that for frequencies $\mathcal{O}$(MHz), the resulting signal could be even 6 or 7 orders of magnitude larger than a putative B-mode

---

[16]In the case of running the bounds on r_T range from 0.58 (in the case of the WMAP 5-yr data alone) to 0.54 if we combine the WMAP data with the large-scale structure data and with the supernova data.

TABLE II. The change in determination of the parameters of the tensor background for three different choices of cosmological data sets.

Data	r_T	n_s	Ω_Λ	Ω_{M0}
WMAP5 alone	<0.43	0.986 ± 0.22	$0.770^{+0.033}_{-0.032}$	$0.230^{0.032}_{-0.033}$
WMAP5 + ACBAR	<0.40	$0.985^{0.019}_{-0.020}$	0.767 ± 0.032	0.233 ± 0.032
WMAP5 + LSS + SN	<0.20	0.968 ± 0.015	0.725 ± 0.015	0.275 ± 0.015
WMAP5 + CMB data	<0.36	0.979 ± 0.020	0.775 ± 0.032	0.225 ± 0.032
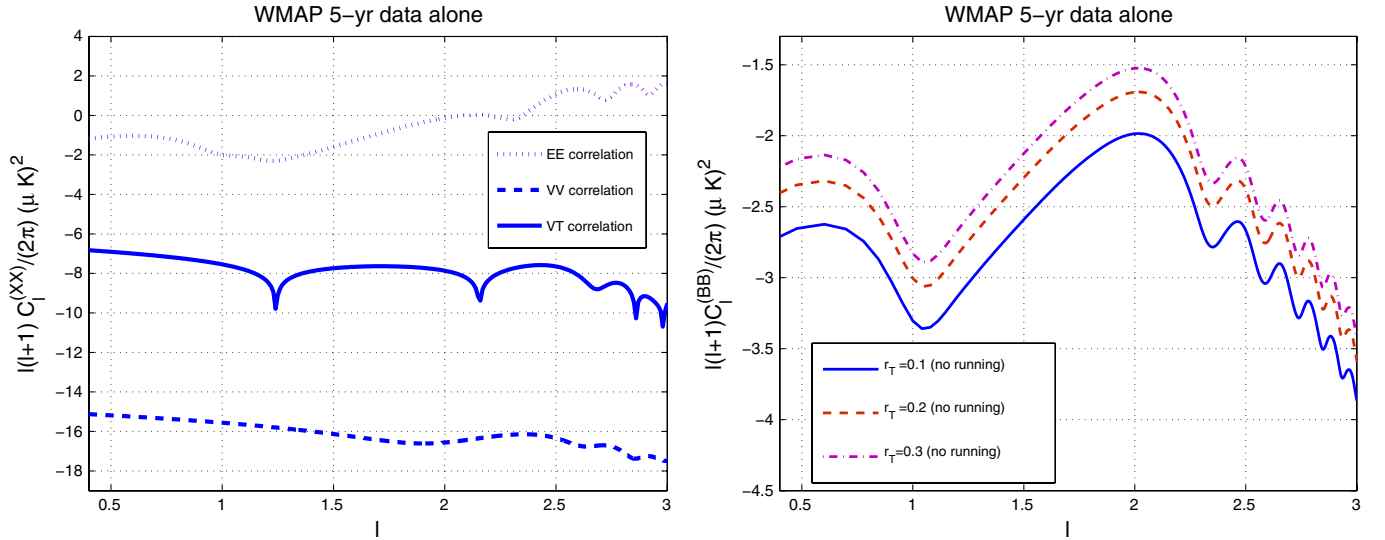
FIG. 5 (color online). The *VV* and *VT* angular power spectra are compared with other polarization signals arising in the ΛCDM paradigm and in its neighboring extensions.

signal from gravitational lensing which is between 10^{-8} and 10^{-6} $(\mu K)^2$.

V. CONCLUDING CONSIDERATIONS

In this paper it has been argued that the presence of a large-scale magnetic field prior to equality can affect the photon-electron and the photon-ion scattering. In this process the radiation becomes circularly polarized and the induced *VV* and *VT* angular power spectra have been computed. The analysis reported in this paper has to be regarded as very preliminary. Indeed the considerations reported here can be refined both at the theoretical as well as at the more observational level. At the same time this investigation certainly opens the way for a more direct use of the circular polarization as a specific diagnostic of predecoupling magnetism. The reported results might also be regarded as a modest spur for those observers and experimenters whose aim is a direct measurement (or a plausible upper limit) on the circular dichroism of the cosmic microwave background.

ACKNOWLEDGMENTS

APPENDIX A: DERIVATION OF THE SCATTERING MATRIX

In a conformally flat background geometry characterized by a metric tensor $g_{\mu\nu}(\tau) = a^2(\tau)\eta_{\mu\nu}$ the electron-ion plasma can be described by the well-known set of two-fluid equations (see, e.g., [57,96]):

$$\vec{\nabla} \cdot \vec{E} = 4\pi e(n_i - n_e), \qquad \vec{\nabla} \cdot \vec{B} = 0 \qquad (A1)$$

$$\vec{\nabla} \times \vec{B} = 4\pi e(n_i\vec{v}_i - n_e\vec{v}_e) + \frac{\partial \vec{E}}{\partial \tau},$$
$$\vec{\nabla} \times \vec{E} = -\frac{\partial \vec{B}}{\partial \tau}, \qquad (A2)$$

where the electromagnetic fields as well as the concentrations of electrons and ions are comoving, i.e.

$$\vec{B}(\vec{x}, \tau) = a^2(\tau)\vec{\mathcal{B}}(\vec{x}, \tau), \qquad \vec{E}(\vec{x}, \tau) = a^2(\tau)\vec{\mathcal{E}}(\vec{x}, \tau)$$

$$n_{e,i}(\vec{x}, \tau) = a^3(\tau)\tilde{n}_{e,i}(\vec{x}, \tau). \qquad (A3)$$

The evolution equations of the electron and ion velocities can be written as

$$\frac{d\vec{v}_e}{d\tau} + \mathcal{H}\vec{v}_e = -\frac{e}{m_e a}[\vec{E} + \vec{v}_e \times \vec{B}], \qquad (A4)$$

$$\frac{d\vec{v}_i}{d\tau} + \mathcal{H}\vec{v}_i = \frac{e}{m_p a}[\vec{E} + \vec{v}_p \times \vec{B}], \qquad (A5)$$

where m_e and m_p are, respectively, the electron and the ion masses; the velocities are related, as usual, to the comoving three-momentum $\vec{v}_{e,i} = \vec{q}_{e,i}/\sqrt{q_{e,i}^2 + m_{e,p}^2 a^2}$. The explicit dependence upon the scale factor at the right-hand side of Eqs. (A4) and (A5) arises because the plasma is cold: both electrons and ions are nonrelativistic and the mass dependence breaks explicitly the Weyl invariance of the whole system already at the level of the Vlasov-Landau equations for the distribution function [57,96]. Finally, in Eqs. (A4) and (A5) $\mathcal{H} = a'/a$ enters directly the Friedmann-Lemaître equations:

$$\mathcal{H}^2 = \frac{8\pi G}{3} a^2 \rho_t, \qquad \mathcal{H}^2 - \mathcal{H}' = 4\pi G a^2 (p_t + \rho_t), \qquad (A6)$$

where ρ_t and p_t denote the total energy density and the total pressure while the prime stands for a derivation with respect to the conformal time coordinate τ. Since the electron and ion concentrations are comoving, they simply obey the following pair of equations

$$n_e' + \vec{\nabla} \cdot (n_e \vec{v}_e) = 0, \qquad n_i' + \vec{\nabla} \cdot (n_i \vec{v}_i) = 0. \qquad (A7)$$

Further details on the description of globally neutral plasma in Friedmann-Robertson-Walker backgrounds can be found, for instance, in [10,33,34,96] (see also [90,91] for earlier results).

The purpose is now to derive the components of the scattering matrix $\mathcal{S}_{ij}(\omega, \mu, \varphi, \mu', \varphi')$ introduced in Eq. (2.3). In the dipole approximation [1], the outgoing electric field can be written as:

$$\vec{E}^{\text{out}}(\vec{x}, \tau) = \frac{1}{rn_0}\left[\hat{r} \times \hat{r} \times \frac{d\vec{J}}{d\tau}\right], \qquad (A8)$$

where

$$\vec{J}(\vec{x}, \tau) = e(n_i \vec{v}_i - n_e \vec{v}_e) = en_0(\vec{v}_i - \vec{v}_e); \qquad (A9)$$

the quantity $n_0 = n_e = n_i$ denotes the common value of the (comoving) electron and ion concentrations. In components the outgoing electric field can be written as

$$E_k = \frac{1}{n_0 r}[(\vec{J}' \cdot \hat{r})\hat{r}_k - J_k'], \qquad (A10)$$

where the prime denotes, as usual, a derivation with respect to the conformal time coordinate. The maximum of the microwave background arises today for typical photon energies of the order of 10^{-3} eV corresponding to a typical wavelength of the mm. At the time of decoupling (i.e. $z_{\text{dec}} \simeq 1089$ according to [22–24]) the wavelength of the radiation was of the order of 10^{-3} mm $\simeq \mu$m. Since the magnetic field we are interested in is inhomogeneous on a much larger length scale we can use the guiding center approximation [51] stipulating that

$$B_i(\vec{x}, \tau) \simeq B_i(\vec{x}_0, \tau) + (x^j - x_0^j)\partial_j B_i + \cdots \qquad (A11)$$

where the ellipses stand for the higher orders in the gradients leading, both, to curvature and drift corrections which will be neglected throughout. Fixing a local coordinate system with three orthogonal axes $\hat{x}$, $\hat{y}$ and $\hat{z}$ the components of the accelerations for the electrons are

$$a_x^{(e)} = -\frac{\omega_{pe}^2}{4\pi n_0 a[1 - f_e^2(\omega)]}[E_x - if_e(\omega)E_y],$$

$$a_x^{(i)} = \frac{\omega_{pi}^2}{4\pi n_0 a[1 - f_i^2(\omega)]}[E_x - if_e(\omega)E_y],$$

$$a_y^{(e)} = -\frac{\omega_{pe}^2}{4\pi n_0 a[1 - f_e^2(\omega)]}[E_y + if_e(\omega)E_y],$$

$$a_y^{(i)} = \frac{\omega_{pi}^2}{4\pi n_0 a[1 - f_i^2(\omega)]}[E_y + if_e(\omega)E_y], \qquad (A12)$$

$$a_z^{(e)} = -\frac{\omega_{pe}^2}{4\pi n_0 a[1 - f_e^2(\omega)]}E_z,$$

$$a_z^{(i)} = \frac{\omega_{pi}^2}{4\pi n_0 a[1 - f_i^2(\omega)]}E_z$$

where $f_{e,i} = \omega_{Be,i}/\omega$; $\omega_{Be,i}$ and $\omega_{pe,i}$ are, respectively, the Larmor and the plasma frequencies either of the electrons or of the ions [see Eqs. (2.27) and (2.28)]. The magnetic field is oriented along the z axis and only the lowest order in the gradient expansion is kept. Of course, as it is well known, higher order will induce both gradient drifts as well as curvature drifts (see, e.g. [51]). We consider these terms to be negligible in the first approximation. Here we are interested in the scattering of electrons and photons not in the stellar atmosphere but rather at the decoupling time when the physical wavelength of the photons is minute in comparison with the inhomogeneity scale of the magnetic field which is of the order of the Hubble radius and even larger [33,34]. The guiding center approximation is pretty robust as far as the magnetized scattering in concerned. For sufficiently small angular scales (i.e. $\ell \gg 100$) the radial direction, in spherical coordinates, coincide (approximately) with the $\hat{z}$ direction. For this reason, in some related paper the modulus of the magnetic field has been taken as $B = \hat{z} \cdot \vec{B} \simeq \hat{n} \cdot \vec{B}$ where the last approximate equality follows in the limit of small angular scales. In

the limit $\ell \gg 100$ the two-sphere actually degenerate into a plane and this is the reason why one can trade the spherical decomposition for the plane wave expansion.

It is also possible to write the difference of the accelerations of electrons and ions, namely, $\vec{A} = (\vec{a}^{(e)} - \vec{a}^{(i)})$ whose components in the local frame are

$$A_x = -\frac{\omega_{pe}^2}{4\pi n_0 a[1 - f_e^2(\omega)]}[\Lambda_1(\omega)E_x - if_e(\omega)\Lambda_2(\omega)E_y],$$
(A13)

$$A_y = -\frac{\omega_{pe}^2}{4\pi n_0 a[1 - f_e^2(\omega)]}[\Lambda_1(\omega)E_y + if_e(\omega)\Lambda_2(\omega)E_x],$$
(A14)

$$A_z = -\frac{\omega_{pe}^2}{4\pi n_0 a[1 - f_e^2(\omega)]}\Lambda_3(\omega)E_z,$$
(A15)

where $\Lambda_1(\omega)$, $\Lambda_2(\omega)$ and $\Lambda_3(\omega)$ have already been defined in Eqs. (2.23)–(2.25). To compute the elements of the scattering matrix it is preferable to pass from the Cartesian components of the incident electric fields to the polar components; the relation between the fields in the two basis is given by:

$$E_x = E'_\vartheta \cos\vartheta' \cos\varphi' - \sin\varphi' E'_\varphi,$$
(A16)

$$E_y = E'_\vartheta \cos\vartheta' \sin\varphi' + \cos\varphi' E'_\varphi,$$
(A17)

$$E_z = -\sin\vartheta' E'_\vartheta.$$
(A18)

To avoid a proliferation of superscripts in the intermediate expressions the ingoing electric fields E'_ϑ and E'_φ are renamed as E_1 and E_2, i.e.

$$E_1 = E'_\vartheta, \qquad E_2 = E'_\varphi.$$
(A19)

Using Eq. (A12) the scattered electric field, in the dipole approximation, become

$$\vec{E} = E_\vartheta \hat{\vartheta} + E_\varphi \hat{\varphi},$$
(A20)

where recalling the notations of Eqs. (2.23)–(2.26)

$$E_\vartheta(\omega, \mu, \mu', \varphi, \varphi') = \frac{r_e}{r}\{[\zeta(\omega)\mu(\mu'E_1\cos(\varphi' - \varphi) - E_2\sin(\varphi' - \varphi)) - \sqrt{1 - \mu^2}\sqrt{1 - \mu'^2}\Lambda_3(\omega)E_1]$$
$$- i\Lambda_2(\omega)f_e(\omega)\zeta\mu[\mu'E_1\sin(\varphi' - \varphi) + E_2\cos(\varphi' - \varphi)]\},$$
(A21)

$$E_\varphi(\omega, \mu, \mu', \varphi, \varphi') = \frac{r_e}{r}\{\zeta(\omega)\Lambda_1(\omega)[\mu'E_1\sin(\varphi' - \varphi) + E_2\cos(\varphi' - \varphi)]$$
$$+ if_e(\omega)\Lambda_2(\omega)\zeta(\omega)[\mu'E_1\cos(\varphi' - \varphi) - E_2\sin(\varphi' - \varphi)]\}.$$
(A22)

Thus, collecting the different factors and rearranging the final expressions we shall have that the scattered electric fields can be written as

$$E_\vartheta(\omega, \mu, \mu', \varphi, \varphi') = \frac{r_e}{r}[AE_1 + BE_2], \qquad E_\varphi(\omega, \mu, \mu', \varphi, \varphi') = \frac{r_e}{r}[CE_1 + DE_2],$$
(A23)

where

$$A(\omega, \mu, \mu', \varphi, \varphi') = \zeta(\omega)\mu\mu'\cos(\varphi' - \varphi) - \sqrt{1 - \mu^2}\sqrt{1 - \mu'^2}\Lambda_3(\omega) - i\Lambda_2(\omega)f_e(\omega)\zeta(\omega)\mu\mu'\sin(\varphi' - \varphi)$$
(A24)

$$B(\omega, \mu, \mu', \varphi, \varphi') = -\zeta(\omega)\mu\sin(\varphi' - \varphi) - i\Lambda_2(\omega)f_e(\omega)\zeta(\omega)\mu\cos(\varphi' - \varphi),$$
(A25)

$$C(\omega, \mu, \mu', \varphi, \varphi') = \mu'\zeta(\omega)\Lambda_1(\omega)\sin(\varphi' - \varphi) + if_e(\omega)\Lambda_2(\omega)\zeta(\omega)\mu'\cos(\varphi' - \varphi),$$
(A26)

$$D(\omega, \mu, \mu', \varphi, \varphi') = \zeta(\omega)\Lambda_1(\omega)\cos(\varphi' - \varphi) - if_e(\omega)\Lambda_2(\omega)\zeta(\omega)\sin(\varphi' - \varphi).$$
(A27)

The Stokes parameters of the scattered radiation can be related to the Stokes parameters of the incident radiation in terms of the appropriate scattering matrix $\mathcal{S}$. As already mentioned in connection with Eq. (2.3), arranging the outgoing and the ingoing Stokes parameters in a pair of column vectors

$$\mathcal{I}_{\text{out}} = (I_\vartheta, I_\varphi, U, V), \qquad \mathcal{I}_{\text{in}} = (I_1, I_2, U', V'),$$
(A28)

the outgoing Stokes parameters are given as $\mathcal{I}_{\text{out}} = \mathcal{S}\mathcal{I}_{\text{in}}$,

where the various components of $\mathcal{S}$ are

$$\mathcal{S}_{11} = \frac{r_e^2}{r^2}|A|^2, \qquad \mathcal{S}_{12} = \frac{r_e^2}{r^2}|B|^2,$$

$$\mathcal{S}_{13} = \frac{r_e^2}{2r^2}(A^*B + B^*A), \qquad \mathcal{S}_{14} = i\frac{r_e^2}{2r^2}(A^*B - B^*A),$$
(A29)

$$\mathcal{S}_{21} = \frac{r_e^2}{r^2}|C|^2, \qquad \mathcal{S}_{22} = \frac{r_e^2}{r^2}|D|^2,$$

$$\mathcal{S}_{23} = \frac{r_e^2}{2r^2}(C^*D + D^*C), \qquad \mathcal{S}_{24} = i\frac{r_e^2}{2r^2}(C^*D - D^*C),$$

$$\text{(A30)}$$

$$\mathcal{S}_{31} = \frac{r_e^2}{r^2}(A^*C + AC^*),$$

$$\mathcal{S}_{32} = \frac{r_e^2}{r^2}(B^*D + D^*B),$$

$$\text{(A31)}$$

$$\mathcal{S}_{33} = \frac{r_e^2}{2r^2}(A^*D + AD^* + BC^* + B^*C),$$

$$\mathcal{S}_{34} = \frac{ir_e^2}{2r^2}(A^*D - AD^* + BC^* - B^*C),$$

$$\mathcal{S}_{41} = \frac{ir_e^2}{r^2}(AC^* - A^*C),$$

$$\mathcal{S}_{42} = \frac{ir_e^2}{r^2}(BD^* - B^*D),$$

$$\text{(A32)}$$

$$\mathcal{S}_{43} = \frac{ir_e^2}{2r^2}(AD^* - A^*D + BC^* - B^*C),$$

$$\mathcal{S}_{44} = \frac{r_e^2}{2r^2}(A^*D + AD^* - B^*C - BC^*).$$

Using Eqs. (A24)–(A27) inside Eqs. (A29) and (A32) the various matrix elements can be readily obtained in explicit terms and have been reported from Eq. (2.7) to Eq. (2.22).

APPENDIX B: DETAILS ON THE DERIVATION OF THE SOURCE TERMS

It is appropriate to give a few details on the derivation of the source terms reported in Eqs. (2.42)–(2.44). Using the results of Eq. (2.41) the source terms of Eqs. (2.31)–(2.34) can be rewritten in explicit terms as

$$
\begin{aligned}
C_I(\omega, \mu) &= \frac{3}{16}\{2\Lambda_3(\omega)(1 - \mu^2)Z_1 + \zeta^2(\omega)[\mu^2 + \Lambda_1^2(\omega) + f_e^2(\omega)\Lambda_2^2(\omega)(1 + \mu^2)]Z_2 \\
&\quad + [2\Lambda_3(\omega)(1 - \mu^2) - \zeta^2(\omega)(\mu^2(1 + f_e^2(\omega)\Lambda_2^2(\omega)) + \Lambda_1^2(\omega) + f_e^2(\omega)\Lambda_2^2(\omega))]Z_3 \\
&\quad + 4f_e^2(\omega)\zeta^2(\omega)\Lambda_2(\omega)(\mu^2 + \Lambda_1)Z_4\}, \\
C_Q(\omega, \mu) &= \frac{3}{16}\{2\Lambda_3(\omega)(1 - \mu^2)Z_1 - \zeta^2(\omega)[\Lambda_1^2(\omega) - \mu^2 + f_e^2(\omega)\Lambda_2^2(\omega)(1 - \mu^2)]Z_2 \\
&\quad + [2\Lambda_3(\omega)(1 - \mu^2) - \zeta^2(\omega)(\mu^2 - \Lambda_1^2(\omega) - f_e^2(\omega)\Lambda_2^2(\omega)(1 - \mu^2))]Z_3 \\
&\quad + 4f_e^2(\omega)\zeta^2(\omega)\Lambda_2(\omega)(\mu^2 - \Lambda_1(\omega))Z_4\}. \\
C_V(\omega, \mu) &= \frac{3}{8}\{\mu\zeta^2(\omega)\Lambda_2(\omega)(\Lambda_1(\omega) + 1)[Z_2 - Z_3] + 2\mu\zeta^2(\omega)[\Lambda_1(\omega) + f_e^2(\omega)\Lambda_2^2(\omega)]Z_4\},
\end{aligned}
$$

$$\text{(B1)}$$

where the four quantities Z_i with $i = 1, 2, 3, 4$ denote the integral of the various brightness perturbations, i.e.

$$Z_1 = \int_{-1}^{1} d\mu'(1 - \mu'^2)\Delta_I d\mu' = \frac{4}{3}[\Delta_{I0} + \Delta_{I2}],$$

$$Z_2 = \int_{-1}^{1} d\mu'(1 + \mu'^2)\Delta_I d\mu', = \frac{8}{3}\Delta_{I0} - \frac{4}{3}\Delta_{I2},$$

$$Z_3 = \int_{-1}^{1} d\mu'(1 - \mu'^2)\Delta_Q d\mu' = \frac{4}{3}[\Delta_{Q0} + \Delta_{Q2}],$$

$$Z_4 = \int_{-1}^{1} \mu'\Delta_V = -2i\Delta_{V1}. \qquad \text{(B2)}$$

To derive Eq. (B2) the standard multipole expansion for the brightness perturbations has been assumed, i.e.

$$\Delta_X(\hat{n}, \tau) = \sum_\ell (-i)^\ell (2\ell + 1)\Delta_{X\ell}P_\ell(\mu). \qquad \text{(B3)}$$

Using the explicit expressions of Eq. (B2) inside Eq. (B1), the expressions reported in Eqs. (2.42)–(2.44) are quickly recovered.

 [1] J. D. Jackson, *Classical Electrodynamics* (Wiley, New York, 1975).
 [2] S. Chandrasekhar, *Radiative Transfer* (Dover, New York, 1966).
 [3] A. Peraiah, *An Introduction to Radiative Transfer* (Cambridge University Press, Cambridge, England, 2001).
 [4] E. T. Newman and R. Penrose, J. Math. Phys. (N.Y.) **7**, 863 (1966).
 [5] J. N. Goldberg *et al.*, J. Math. Phys. (N.Y.) **8**, 2155 (1967).
 [6] L. C. Biedenharn and J. D. Louck, *Angular Momentum in Quantum Physics* (Addison-Wesley, Reading, MA, 1981).
 [7] D. A. Varshalovich, A. N. Moskalev, and V. K. Khersonskii, *Quantum Theory of Angular Momentum* (World Scientific, Singapore, 1988).
 [8] J. J. Sakurai, *Modern Quantum Mechanics* (Addison-Wesley, New York, 1985).
 [9] M. Giovannini, Int. J. Mod. Phys. D **13**, 391 (2004).
 [10] M. Giovannini, Classical Quantum Gravity **23**, R1 (2006).
 [11] S. K. Solanki, B. Inhester, and M. Schüssler, Rep. Prog. Phys. **69**, 563 (2006).
 [12] R. Illing, D. Landman, and D. L. Mickey Astron. Astrophys. **35**, 327 (1974).
 [13] L. Auer and J. N. Heasley, Astron. Astrophys. **64**, 67 (1978).
 [14] K. Ichimoto *et al.*, Astron. Astrophys. **481**, L9 (2008).
 [15] V. M. Grigorjev and J. M. Katz, Sol. Phys. **42**, 21 (1975).
 [16] A. G. Pacholczyk and T. L. Swihart, Astrophys. J. **150**, 647 (1967).
 [17] V. N. Sazonov, Zh. Eksp. Teor. Fiz. **56**, 1065 (1969) [Sov. Phys. JETP **29**, 578 (1969)].
 [18] A. G. Pacholczyk and T. L. Swihart, Astrophys. J. **161**, 415 (1970).
 [19] T. Jones and A. O'Dell, Astrophys. J. **214**, 522 (1977); **215**, 236 (1977).
 [20] D. Lai and W. C. G. Ho, Astrophys. J. **588**, 962 (2003).
 [21] A. Cooray, A. Melchiorri, and J. Silk, Phys. Lett. B **554**, 1 (2003).
 [22] G. Hinshaw *et al.* (WMAP Collaboration), Astrophys. J. Suppl. Ser. **180**, 225 (2009).
 [23] J. Dunkley *et al.* (WMAP Collaboration), Astrophys. J. Suppl. Ser. **180**, 306 (2009).
 [24] E. Komatsu *et al.* (WMAP Collaboration), Astrophys. J. Suppl. Ser. **180**, 330 (2009).
 [25] D. N. Spergel *et al.* (WMAP Collaboration), Astrophys. J. Suppl. Ser. **170**, 377 (2007).
 [26] L. Page *et al.* (WMAP Collaboration), Astrophys. J. Suppl. Ser. **170**, 335 (2007).
 [27] C. Pryke *et al.* (QUaD Collaboration), Astrophys. J. **692**, 1247 (2009).
 [28] E. Y. Wu *et al.* (QUaD Collaboration), Phys. Rev. Lett. **102**, 161302 (2009).
 [29] P. G. Castro *et al.* (QUaD Collaboration), Astrophys. J. **701**, 857 (2009).
 [30] R. B. Friedman *et al.* (QUaD Collaboration), Astrophys. J. **700**, L187 (2009).
 [31] C. l. Kuo *et al.* (ACBAR Collaboration), Astrophys. J. **600**, 32 (2004).
 [32] C. L. Kuo *et al.*, Astrophys. J. **664**, 687 (2007); C. L. Reichardt *et al.*, Astrophys. J. **694**, 1200 (2009).
 [33] M. Giovannini, Phys. Rev. D **79**, 121302 (2009).
 [34] M. Giovannini, Phys. Rev. D **79**, 103007 (2009).
 [35] M. Giovannini, Report No. CERN-PH-TH-2009-117.
 [36] M. Giovannini and K. E. Kunze, Phys. Rev. D **79**, 063007 (2009).
 [37] G. Sironi (private communications).
 [38] G. Sironi, M. Limon, G. Marcellino, G. Bonelli, M. Bersanelli, and G. Conti, Astrophys. J. **357**, 301 (1990).
 [39] G. Sironi, G. Bonelli, and M. Limon, Astrophys. J. **378**, 550 (1991).
 [40] M. Zannoni *et al.*, Astrophys. J. **688**, 12 (2008).
 [41] M. Gervasi *et al.*, Astrophys. J. **688**, 24 (2008).
 [42] A. Tartari *et al.*, Astrophys. J. **688**, 32 (2008).
 [43] E. Fermi and S. Chandrasekhar, Astrophys. J. **118**, 113 (1953).
 [44] E. Fermi and S. Chandrasekhar, Astrophys. J. **118**, 116 (1953).
 [45] S. Chandrasekhar and P. C. Kendall, Astrophys. J. **126**, 457 (1957).
 [46] S. Chandrasekhar and L. Woltjer, Proc. Natl. Acad. Sci. U.S.A. **44**, 285 (1958).
 [47] L. Woltjer, Proc. Natl. Acad. Sci. U.S.A. **44**, 489 (1958).
 [48] K. Subramanian and J. D. Barrow, Phys. Rev. Lett. **81**, 3575 (1998).
 [49] K. Subramanian and J. D. Barrow, Mon. Not. R. Astron. Soc. **335**, L57 (2002).
 [50] K. Subramanian, T. R. Seshadri, and J. D. Barrow, Mon. Not. R. Astron. Soc. **344**, L31 (2003).
 [51] H. Alfvén and C.-G. Fälthammer, *Cosmical Electrodynamics* (Clarendon, Oxford, 1963), 2nd ed.
 [52] B. Whitney, Astrophys. J. Suppl. Ser. **75**, 1293 (1991).
 [53] K. C. Chou, Astrophys. Space Sci. **121**, 333 (1986).
 [54] M. Giovannini, *A Primer on the Physics of the Cosmic Microwave Background* (World Scientific, Singapore, 2008).
 [55] M. Zaldarriaga and U. Seljak, Phys. Rev. D **55**, 1830 (1997).
 [56] M. Zaldarriaga and D. D. Harari, Phys. Rev. D **52**, 3276 (1995).
 [57] M. Giovannini, Phys. Rev. D **71**, 021301 (2005); M. Giovannini and K. E. Kunze, Phys. Rev. D **78**, 023010 (2008).
 [58] A. Kosowsky and A. Loeb, Astrophys. J. **469**, 1 (1996).
 [59] D. D. Harari, J. D. Hayward, and M. Zaldarriaga, Phys. Rev. D **55**, 1841 (1997).
 [60] M. Giovannini, Phys. Rev. D **56**, 3198 (1997).
 [61] C. Scoccola, D. Harari, and S. Mollerach, Phys. Rev. D **70**, 063003 (2004).
 [62] G. Chen *et al.*, Astrophys. J. **611**, 655 (2004).
 [63] P. D. Naselsky, L. Y. Chiang, P. Olesen, and O. V. Verkhodanov, Astrophys. J. **615**, 45 (2004).
 [64] T. Souradeep, A. Hajian, and S. Basak, New Astron. Rev. **50**, 889 (2006).
 [65] A. Hajian and T. Souradeep, Phys. Rev. D **74**, 123521 (2006).
 [66] M. Giovannini, Phys. Rev. D **58**, 124027 (1998).
 [67] M. Giovannini, Phys. Rev. D **61**, 063004 (2000).
 [68] M. Giovannini, Phys. Rev. D **61**, 063502 (2000).
 [69] C. J. Copi, F. Ferrer, T. Vachaspati, and A. Achucarro, Phys. Rev. Lett. **101**, 171302 (2008).
 [70] A. Diaz-Gil, J. Garcia-Bellido, M. G. Perez, and A. Gonzalez-Arroyo, J. High Energy Phys. 07 (2008) 043.

[71] C. Adam, B. Muratori, and C. Nash, Phys. Rev. D **62**, 105027 (2000).

[72] A. Ayala, G. Piccinelli, and G. Pallares, Phys. Rev. D **66**, 103503 (2002).

[73] L. Campanelli and M. Giannotti, Phys. Rev. Lett. **96**, 161302 (2006).

[74] K. Bamba, C. Q. Geng, and S. H. Ho, Phys. Lett. B **664**, 154 (2008); K. Bamba, Phys. Rev. D **74**, 123504 (2006).

[75] T. Kahniashvili, New Astron. Rev. **50**, 1015 (2006).

[76] J. M. Beckers and E. H. Schröter, Sol. Phys. **4**, 142 (1968).

[77] D. Soltau, Astron. Astrophys. **317**, 586 (1997).

[78] E. Valtaoja, Astrophys. Space Sci. **100**, 227 (1984).

[79] R. Böstrom, Astrophys. Space Sci. **22**, 353 (1973).

[80] C. Chu and T. Ozawa, Phys. Rev. Lett. **48**, 837 (1982); **58**, 424 (1987).

[81] H. Zaghloul, K. Volk, and A. Buckmaster, Phys. Rev. Lett. **58**, 423 (1987).

[82] N. A. Salingaros, Phys. Rev. A **45**, 8811 (1992).

[83] H. Murata, J. Fluid Mech. **100**, 31 (1980).

[84] Z. Yoshida, J. Plasma Phys. **45**, 481 (1991).

[85] R. Jackiw and S. Y. Pi, Phys. Rev. D **61**, 105015 (2000).

[86] E. Bertschinger, arXiv:astro-ph/9506070; C. P. Ma and E. Bertschinger, Astrophys. J. **455**, 7 (1995).

[87] M. Abramowitz and I. A. Stegun, *Handbook of Mathematical Functions* (Dover, New York, 1972).

[88] A. Erdelyi, W. Magnus, F. Obehettinger, and F. Tricomi, *Higher Trascendental Functions* (Mc Graw-Hill, New York, 1953).

[89] M. Giovannini, Report No. CERN-PH-TH/2009-171.

[90] M. Giovannini, Phys. Rev. D **74**, 063002 (2006).

[91] M. Giovannini, PMC Phys. A **1**, 5 (2007).

[92] R. A. Sunyaev and Y. B. Zeldovich, Astrophys. Space Sci. **7**, 3 (1970).

[93] B. Jones and R. Wyse, Astron. Astrophys. **149**, 144 (1985).

[94] P. Naselsky and I. Novikov, Astrophys. J. **413**, 14 (1993).

[95] H. Jorgensen, E. Kotok, P. Naselsky, and I. Novikov, Astron. Astrophys. **294**, 639 (1995).

[96] M. Giovannini and N. Q. Lan, Phys. Rev. D **80**, 027302 (2009).